POLITECNICO DI TORINO

LAUREA MAGISTRALE

In Ingegneria Civile

Modelling and Parametric Identification of the Unstable Behaviour of Fibre-reinforced Materials: A New Computational Code

Candidate:

Lorenzo Brocchi s296023

Supervisors:

Prof. Giuseppe Lacidogna (POLITO)

Prof. Alberto Carpinteri (STU)

Prof. Federico Accornero (STU)

a.a. 2024/2025

Contents

Alla mia famiglia ed ai miei amici

Homo sum, humani nihil a me alienum puto.

Publio Terenzio Afro, Heautontimorumenos 165 a.c.

MADE WITH LOVE

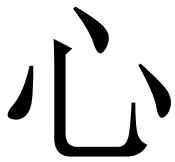

Acknowledgments

My Master Thesis has been completely performed at the Shantou University premises.

I want to thank sincerely my Professors Alberto Carpinteri and Federico Accornero for giving the opportunity to spend a full semester in China. Moreover, I want to thank Mrs. Maria Giulia and Mrs. Elena that made me feel like home from day one in Guangdong.

A special acknowledgement to Mr. Dongxi and Mrs. Calif, from Shantou University, which guided me at the very beginning through all the bureaucratic issues.

To my Chinese friend Zayne, wishing that his semester in Italy can be as wonderful as mine at STU.

Last but not least, to all the members of Sung Pu Three House, for the joyful time spent together: to Alice the queen of Thailand, to Dylan Davis O`Flanagan, Jerine, Ayana, Michelle, Pau, Feng and all the others.

Abstract

An accurate model for prismatic specimen subjected to bending action is crucial both for prediction and design decision making. The new Updated Bridged Crack Model 2.0 represents a precise tool, which let final users, such as scholars and engineers, to model in advanced beams made of concrete, polymer, metal and ceramic matrices both fibre-reinforced and plain. The study performed underline the validity of the MATLAB software in identifying fibre-reinforced concrete, hybrid-reinforced concrete, simple steel-bar reinforced concrete and plain concrete with astonishing velocity and precision performances. A new perspective is explained hereafter, by giving successful preliminary example over new materials with usage spread in different fields of engineering: civil, aerospace and nuclear. These results lead UBCM 2.0 to cover a wider range of applicability, letting it be universal in the meandering of flexural modeling.

Keywords: Fracture mechanics, Reinforced concrete, Fibre-reinforced concrete, Hybrid-reinforced concrete, Updated Bridged Crack Model 2.0, Brittleness numbers, Tension stiffening, Fibre-reinforced polymer matrix composites, Fibre-reinforced metal matrix composites, Fibre-reinforced ceramic matrix composites.

Introduction

The new software is described in the following “Updated Bridged Crack Model 2.0”, a debugged and revised version of the well-known UBCM. In the first paragraph is explained the new algorithm, which performs well and tackles the convergence issue related to over-reinforced concrete beams. Furthermore, some numerical and experimental curves are plotted to validate the model; then, 80 simulations are performed to highlight the code’s performances by varying the variable numerical number of fibres and the new parameter, max iterations before convergence as a benchmark is used the time of code’s execution.

The second chapter deals with the pre-peak of both reinforced concrete and hybrid reinforced concrete beams. In this first branch, a phenomenon called Tension-stiffening occurs; the introduction of a new constitutive law let the simulation better approximating experimental results. The parameter “n of tension stiffening” should be identified and quantifies the real yielding crack opening in the beams; this latter depends on slenderness, reinforcement ratio and fibre volume fraction. The decision-making regarding *n* is performed by means a simple K-NN machine learning model, which is able to retrieve reliable value to predict new experimental results. Eventually, 96 simulations are computed to assess the model’s behavior under different situations in terms of execution’s time.

The third and last chapter aims to generalize the model to every kind of fibre-reinforced composite materials. Two new constitutive laws (Softening and Hardening) are introduced to describe every fashion of reinforcement. Despite the lack of information in the scientific papers analyzed; the assumptions made let the model describing smoothly: fibre-reinforced polymer matrix composites (PMC), fibre-reinforced metal matrix composites (MMC) and fibre-reinforced ceramic matrix composites (CMC).

Lastly, the Annex A gathers useful information for the final user to utilize the new Graphical User Interface (GUI) of the UBCM 2.0.

1. The Updated Bridged Crack Model 2.0 (UBCM 2.0)

This first chapter briefly describes the state of the art of the Updated Bridged Crack Model (UBCM) and how the revised version of the code can overcome the convergence problem occurring for over-reinforced concrete beams, also achieving greater results in terms of computation's velocity and readability. Secondly, it threats proper input settings, regarding maximum iteration and numerical number of fibres in the considered cracking cross-section; eventually, it contains numerical curves of Fibre-reinforced Concrete (FRC) from the large test campaign of Prof. Carpinteri and Prof. Accornero research group in Shantou University and FRC experimental curves present in literature, useful to validate the new model.

1.1 State of the art

The Updated Bridged Crack Model (UBCM) uses Fracture Mechanics theory to evaluate the flexural response of Reinforced Concrete (RC), Fibre-reinforced Concrete (FRC) and Hybrid-reinforced Concrete (HRC) beams subjected to monotonically increasing or cycling loads. The novelties of the proposed analysis are the following: the beam element could be considered as two rigid blocks connect by an internal inelastic spring, located in the cracked cross-section; moreover, the computation is driven by imposing a fictitious crack advancement in the critical cross-section, evaluating step-by-step the applied forces and displacements by means Compatibility and Equilibrium equations.

In the forerunner framework of Bridged Crack Model (BCM), presented by Carpinteri [1-2], the concrete matrix is modeled in the framework of Linear Elastic Fracture Mechanics (LEFM), by means an elastic-brittle constitutive law; actually, this approximation doesn't consider the softening branch in tension of the plain concrete, the effectiveness of this hypothesis is given by the fact that the process

zone in between nodes is of infinitesimal depth, in which the material is not able to exert is original behavior. The reinforcement steel-bar is originally modeled as rigid-perfectly plastic; the overall response of the cracked bi-phase element shows a linear hardening branch in the Moment rotation diagram, circumscribing the BCM in the field of Non-linear Fracture Mechanics.

Recently, the fibre reinforcements are introduced in the model to predict the behavior of both FRC and HRC [4]; the shorter steel bars are characterized by softening constitutive laws, in two fashions: Straight steel fibres and Hooked-end steel fibres. According to the authors, Accornero et al. [5], UBCM can investigate the post-cracking behavior of the FRC beams in bending, in addiction, can act as a powerful tool to design HRC, accounting for both minimum steel-fibre reinforcement and minimum steel-bar reinforcement [6]. The analysis is carried on by means of the simple and direct tool of Brittleness number, firstly introduced by Carpinteri [7] in 1981; in the context of UBCM, are considered indeed three Brittleness number: N_P *bar-reinforcement brittleness number,* $N_{P,f}$ *fibre-reinforcement brittleness number* and the N_w *pull-out brittleness number.* By means the calculation of the critical values of the above-mentioned dimensionless quantities is possible to retrieve the minimum amount of both steel-bar reinforcement and fibre-reinforcement.

1.2 The new version of the code

The current version of the code is written and handled in MATLAB environment.

Some programming tools are added to improve the readability and the computation performances of the code. A data gathering system managed through classes, Object Oriented Programming (OOP) is added to the backbone of the code, this could clarify the master code and organize properly the inputs from the user-side. Five classes are created: “concrete”, “reinforcement”, “fibre”, “crosssection” and “test”, gathering data input and performing by means functions the calculations of indirect quantities directly in the class to not burden the master.

In some cases, has been possible to Vectorize some operations, in order to avoid “for-loops”, which are in general not effective and weaken the code, slowing down procedures through useless iterations.

Moreover, the previous version of the code presents a missed *Convergence* check through iterations inside a “while-loop”, this leads to very slow computation procedure, and in the case of over-reinforced beams, it means a percentage of bar-reinforcement close to the maximum value, to not calculate a solution at all. In mathematics and computer science the convergence is related to the fact that different computations made in sequence, should reach a result in a finite amount of time, independently of the path chosen to achieve it. After an extensive numerical analysis, it turned out that the check procedure was not effective and stacked at the fifth decimal cipher; far more precise than the needed one. The issue is solved by adding an iteration counter within the “while-loop”; once the maximum threshold of iteration is reached the program should retrieve a solution. The upper bound introduced is a new user-side input and the setting of the proper value will be deeper treated later in this chapter. In the below figure is reported the revised *Flow-Chart* of the UBCM 2.0 algorithm.

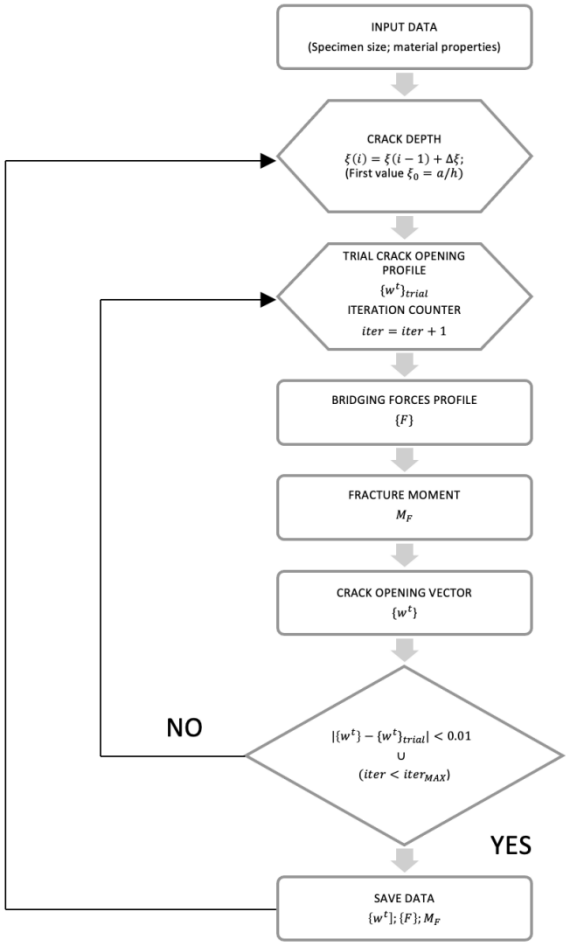

Figure 1: flow-chart UBCM 2.0 algorithm.

This scheme is the revised version of Rubino PhD thesis [8].

As it can be deduced from the Figure 1, this is a Crack Length Control Scheme (CLCS) and its termination coincides with the almost complete disconnection of the beam $a \approx h$, or better in terms of Relative Crack Depth ($\xi = a/h$), as $\xi \approx 0$. After the Loading condition, Three Point Bending Test (3-PBT) or Four Point Bending Test (4-PBT), the Specimen geometry (Beam depth h, Beam thickness t etc..), Material properties and reinforcement characterization are set, the actual crack depth is to be identified as well as the amount of active reinforcing layers m (First iteration: $\xi_0 = \frac{a_0}{h}$; m = 0). Secondly, the local compliances and the trial crack openings profile $\{w^t\}_{trial}$ are calculated, and the iteration counter is initialized.

The subsequent step is to evaluate the Bridging Forces profile $\{F\}$, assuming the fibres and the tensile steel-bar oriented perpendicularly to the crack surface; consequently, the computation of the Fracturing Moment M_F is performed, defined as the bending moment in the cross-section causing the crack advancement (in the framework of LEFM occurs as the Stress Intensity Factor is approaching is critical value: $K_I = K_{IC}$). By means these quantities and the compliances is possible to calculate the vector of Crack Opening Displacement $\{w^t\}$.

This latter should be compared to the trial one and the difference in absolute value should be comprised in between the bounds $[-0.01; +0.01]$. The novelty of UBCM 2.0 is the introduction of another Convergence check, regarding the maximum amount of iteration to reach this condition ($iter < iter_{MAX}$); this prevent the code to be unfeasible for larger amount of steel-bar reinforcement. As one of the checks is met, the data are saved and the crack advances of a quantity $\Delta\xi$. As last remark, it can be stated that the system has $2m+1$ unknowns, m nodal displacements, m nodal forces and the M_F the Fracturing Bending moment. The number of reacting reinforcing layers is a user-side input and some deeper consideration about that are presented later in this chapter.

1.3 Model Validation

In order to ensure the validity of the proposed solution, a part of the numerical curves from the large test campaign of Prof. Carpinteri and Prof. Accornero are here represented, as well as experimental curves found in literature

1.3.1 Numerical Curves

This assessment is useful to test the model, as well as to predict the behavior of the tested specimens. Some of the presented curves could be obtained effectively by UBCM, but as far as the fibre volume increases, and at the same time the number of unknowns, the old version of the model is not able to reach the solution in finite amount of time.

For this campaign that counts almost 500 specimens, 100 are of interest of study for this Master Thesis. The hundred specimens are respectively RC, FRC and HRC concrete beams subjected to 4-PBT displacement driven, with monotonically increase rate as recommended by RILEM [84]. The controlled quantity is the Crack Mouth Opening Displacement (CMOD), which avoids the representation of the catastrophic behavior of brittle specimens and a better characterization of the softening branch. The test machine is MTS with max load equal to 100 tons. As far as the campaign based at Shantou University, Guangdong, China is not yet started, no more information is available. In this paragraph are analyzed 16 FRC beams and 4 Plain Concrete (PC) beams, with constant Slenderness ratio ($\lambda=h/S=6$), material properties and fibre typology; but varying the fibre content, represented as Fibre Volume Fraction V_f expressed in percentage and ranging from 0% (Case of PC) to 0.8%; the scale, depth of the beams (h) from 200 mm to 1600 mm. Here below are reported tables gathering information about specimens in terms of: Concrete Matrix properties and Beam Properties, Fibre typology and properties. The Beam ID is composed in this way: PC stand for Plain Concrete, FRC for Fibre Reinforced Concrete, 20 is the depth of the beam in cm and eventually 0-0.1-..-0.8 indicates the Fibre Volume Fraction in percentage. To be noted is the quantity w_c, which

represents the fibre critical embedded length, its mean value is equal to ¼ of the length of the fibre itself and is the actual reacting length of the single fibre.
In the above Figure 2: 4-PBT scheme.Figure 2 is represented the scheme of the test:

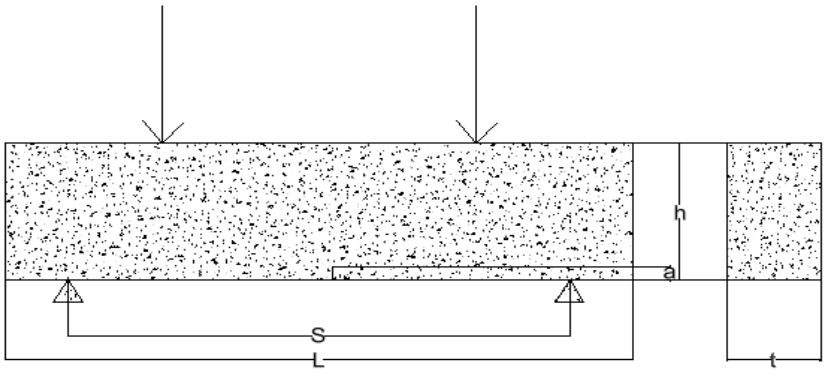

Figure 2: 4-PBT scheme.

CONCRETE MATRIX	
Properties	
E (Young's Modulus) [MPa]	30000
K_{IC} (Fracture Toughness) [MPa mm$^{0.5}$]	30
σ_c(Cubic Compressive Strength) [MPa]	30

Table 1: Concrete matrix properties for the numerical curves.

FIBRE-REINFORCEMENT	
Properties	
Typology [-]	Hooked-End
d_f (fibre diameter) [mm]	0,5
l_f (fibre length) [mm]	30
λ_f (aspect ratio) [-]	60
F_s (Pull-out force) [N]	35
w_c (Critical embedded length) [mm]	7,5

Table 2: Fibre properties for the numerical curves.

Beam ID	Depth *h* [mm]	Thickness *t* [mm]	Span *S* [mm]	Initial crack depth *a* [mm]
PC20	200	200	1200	20
FRC20-0.1	200	200	1200	20
FRC20-0.2	200	200	1200	20
FRC20-0.4	200	200	1200	20
FRC20-0.8	200	200	1200	20
PC40	400	200	2400	40
FRC40-0.1	400	200	2400	40
FRC40-0.2	400	200	2400	40
FRC40-0.4	400	200	2400	40
FRC40-0.8	400	200	2400	40
PC80	800	200	4800	80
FRC80-0.1	800	200	4800	80
FRC80-0.2	800	200	4800	80
FRC80-0.4	800	200	4800	80
FRC80-0.8	800	200	4800	80
PC160	1600	400	9600	160
FRC160-0.1	1600	400	9600	160
FRC160-0.2	1600	400	9600	160
FRC160-0.4	1600	400	9600	160
FRC160-0.8	1600	400	9600	160

Table 3: Prismatic specimen geometry.

Beam ID	Theoretical number of fibres [-]	Numerical number of fibres *m* [-]
PC20	0	0
FRC20-0.1	21	21
FRC20-0.2	43	43
FRC20-0.4	85	85
FRC20-0.8	171	100
PC40	0	0
FRC40-0.1	43	43
FRC40-0.2	85	85
FRC40-0.4	171	100
FRC40-0.8	341	100
PC80	0	0
FRC80-0.1	85	85
FRC80-0.2	171	100
FRC80-0.4	341	100
FRC80-0.8	683	100
PC160	0	0
FRC160-0.1	341	100
FRC160-0.2	683	100
FRC160-0.4	1365	100
FRC160-0.8	2731	100

Table 4: Theoretical vs Numerical number of fibres for numerical curves.

In the above Table 4 are present two quantities, the Theoretical number of fibres and the Numerical number of fibres. The former indicates the right amount of short reinforcement that should be present in the cracked surface at mid span according to volumetric measure; the latter refers to the number of reacting fibres considered in the code m, it can be noted that when the number of theoretical fibres increases significantly, a smooth representation of the curves can be achieved by setting m =100 . Whereas, for the sake of precision when the

theoretical number of fibres is below the threshold, the numerical number is adjusted accordingly.

Then are plotted the numerical curves, mid span deflection δ [mm] versus Load *P* [N] from the *h* = 20 cm to the *h* = 160 cm:

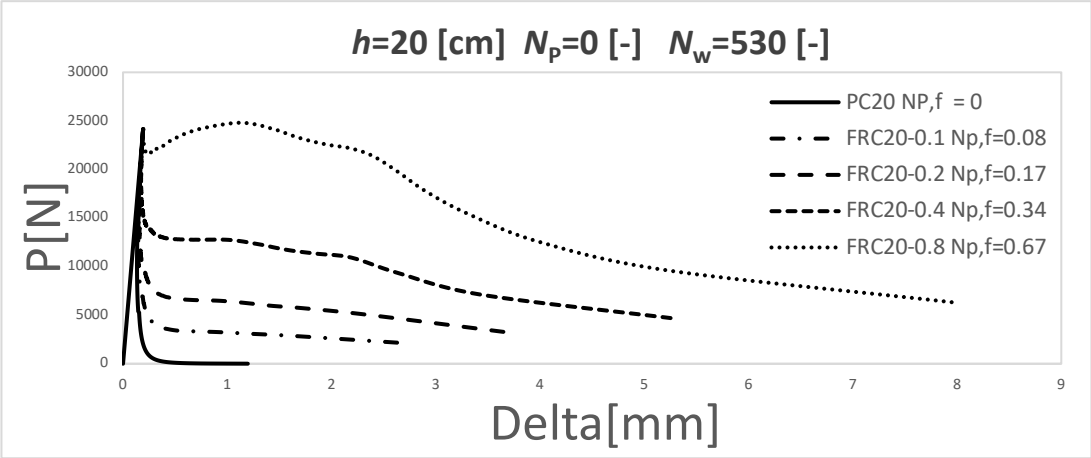

Figure 3: Numerical Curves of beams with 20 cm depth.

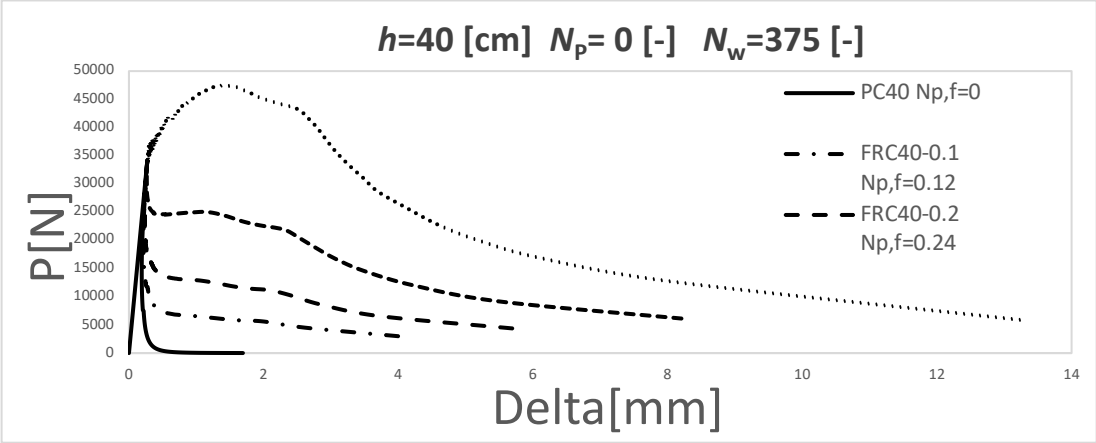

Figure 4: Numerical Curves of beams with 40 cm depth.

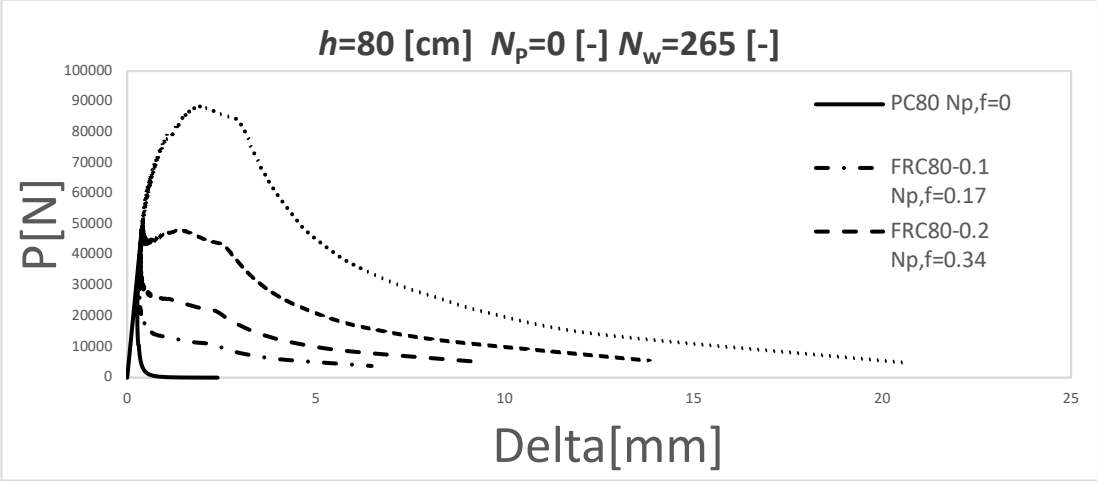

Figure 5: Numerical Curves of beams with 80 cm depth.

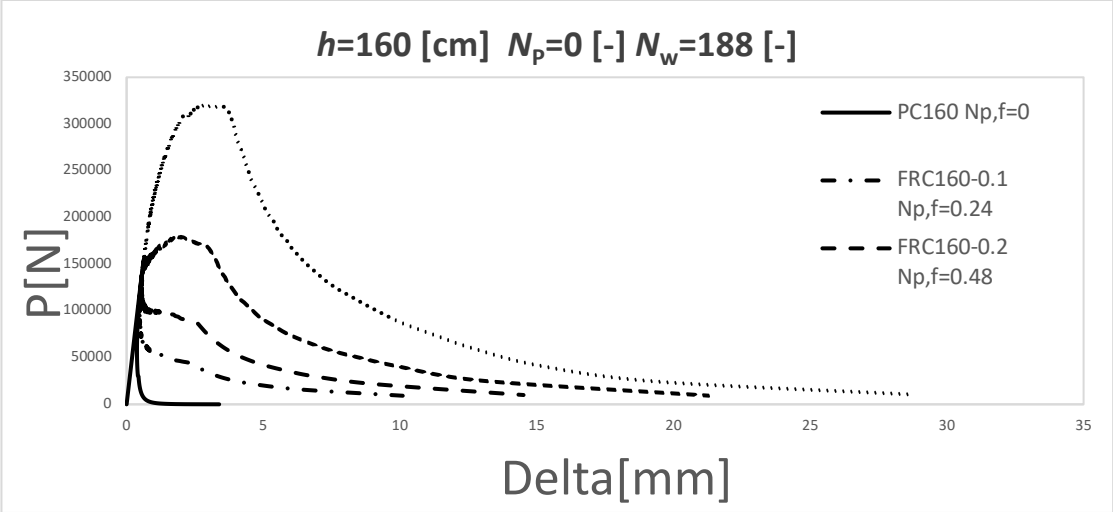

Figure 6: Numerical Curves of beams with 160cm depth.

Now, it`s performed a detailed analysis of the curves based on the Brittleness numbers; they are obtained through the application of the well-known Buckingham Theorem [10].

In the case of a FRC beams, the following functional dependence can be stated:

$$\Pi(M_F, \Theta; K_{IC}, E; V_f, \sigma_s, w_c; b, h, a) = 0 \qquad (Eq.\ 1.1)$$

Where:

- θ : mid-span rotation [rad]

- σ_s: Slippage strength of the single fibre [MPa]

Assuming (K_{IC}, *h)* as independent variables, the (Eq. 1.1) can be rewritten as:

$$\Pi^*\left(\frac{M_F}{K_{IC} b h^{3/2}}, \Theta \frac{E}{K_{IC}} h^{1/2}, V_f \frac{\sigma_s}{K_{IC}} h^{1/2}, \frac{E w_c}{K_{IC} h^{1/2}}, \frac{b}{h}, \frac{a}{h}\right) = 0 \quad \text{(Eq. 1.2)}$$

Here above are present the two Brittleness number governing the behavior of the FRC beams:

- $N_{P,f} = V_f \frac{\sigma_s}{K_{IC}} h^{1/2}$ (Eq. 1.3)

- $N_w = \frac{E w_c}{K_{IC} h^{1/2}}$ (Eq. 1.4)

In (Eq. 1.3) is defined the Fibre-reinforcement brittleness number, depending mainly on the Fibre volume fraction, governing the Beam Bearing capacity in the Post-Crack stage, just after the elastic phase. In (Eq. 1.4) is declared the Pull-out brittleness number, depending on the critical embedded length of fibre, it is responsible of the third stage also known as Pull-out tail which refers to the softening last part of a typical load-mid span deflection plot of FRC beam. Is worthy to note that in this case the Bar-reinforcement brittleness number is equal to zero, as far as no steel-bar reinforcement are present in the FRC specimens, therefore it is not influencing the bearing capacity of the specimens.

In the following table are summed up all the brittleness parameter of the 20 beams:

Beam ID	$N_{P,f}$ [-]	N_w [-]
PC20	0	530
FRC20-0.1	0.08	530
FRC20-0.2	0.17	530
FRC20-0.4	0.34	530
FRC20-0.8	0.67	530
PC40	0	375
FRC40-0.1	0.12	375
FRC40-0.2	0.24	375
FRC40-0.4	0.48	375
FRC40-0.8	0.67	375
PC80	0	265
FRC80-0.1	0.17	265
FRC80-0.2	0.34	265
FRC80-0.4	0.67	265
FRC80-0.8	1.34	265
PC160	0	188
FRC160-0.1	0.24	188
FRC160-0.2	0.48	188
FRC160-0.4	0.95	188
FRC160-0.8	1.90	188

Table 5: Numerical Curves Brittleness parameters.

If the curves are numerical, in the case of $N_{P,f}$ the only varying parameters are the depth and the fibre content; in addiction, considering N_w the only changing parameter is the scale of the specimen, but being gathered at the denominator in this case is worthy to call the influence of h as *Reverted Scale effect*.

Talking about the first group of beams in Figure 3 , their prevalent behavior is softening as far as the scale effect, related to h, and the content of fibre is not enough large to meet the critical situation. It's observable that only FRC20-0.8 has a Fibre-reinforcement brittleness number close to the critical value, owing to the short plastic plateau just after the peak, without further investigation can be considered as the threshold value for the ductile-to-brittle transition. Regarding N_w, in the analyzed context it presents a large value, which corresponds to larger rotational capacity, as far as the curves are tending to different asymptotic values; the influence of Pull-out brittleness number is strong.

In Figure 4, are depicted the group of specimens with 40 cm depth. Only FRC40-0.8 has a Fibre-reinforcement brittleness number such that a pseudo Plastic-hardening behavior is achieved after the Elastic peak. The influence of N_w is still strong and therefore the softening tails are tending to different asymptotic values. The beams of depth 80 cm, in Figure 5, show similar dependency to the brittleness parameters, with FRC80-0.4 perfectly plastic behavior in the second stage and FRC80-0.8 with its pseudo hardening branch. The tails are closer each other but tending to different asymptotes.

Eventually, the largest scale is analyzed in Figure 6: both FRC160-0.4 and FRC160-0.8 have enough fibre content to present, respectively, a perfectly-plastic behavior and pseudo-hardening behavior; the main difference in this case is the influence of the Pull-out brittleness number, being sufficiently small that all the curves in the third stage exhibit an asymptotic trend to zero, or plastic flow at level zero, underlining the loss in rotational capacity as the scale increase; this is an evident result of the reverted scale effects.

1.3.2 Experimental Curves

The last assessment made to validate the model, regards the application of the UBCM 2.0 to experimental curves present in literature, to highlight the adherence of the framework to actual tests.

The first paper under analysis is by Yoo et al. [11]: the study is comparing the performances of textile-reinforced concrete and steel-fibre reinforced concrete (SFRC) under low velocity loading; despite that, the interest of this study is to assess the response of SFRC under static load, subjected to a 4-PBT.

The beam ID is composed in this way: S stands for Steel-fibre reinforcement and 0.5%-..-2% is the fibre volume fraction.

Here above are reported the input properties as reported in the article:

CONCRETE MATRIX	
Properties	
E (Young's Modulus) [MPa]	83415
K_{IC} (Fracture Toughness) [MPa mm$^{0.5}$]	40
σ_c (Cubic Compressive Strength) [MPa]	56.95

Table 6: Concrete Matrix properties of Yoo et al. curves.

FIBRE-REINFORCEMENT	
Properties	
Typology [-]	Hooked-End
d_f (fibre diameter) [mm]	0.5
l_f (fibre length) [mm]	30
λ_f (aspect ratio) [-]	60
F_S (Pull-out force) [N]	75
w_c (Critical embedded length) [mm]	7.5

Table 7: Fibre-reinforcement properties of Yoo et al. curves.

Preceding the representation of the experimental curves, the following mechanical parameters must be properly examined, in the so-called Identification procedure:

- K_{IC}: Fracture toughness, regarding the concrete matrix.

- F_S: Pull-out force of the single fibre, sometimes expressed as $\bar{\sigma}_s$ [MPa] i.e., slippage strength of the fibre.

- w_c: Critical embedded length of the fibre.

Each one of the former quantities free to vary meanwhile the other two are maintained constants. The first one is identified once the Fracturing moment of the numerical results of UBCM 2.0 and the actual one coincides. It`s worthy to note that in the case of this paper, the specimen is unnotched; being M_F function of both relative crack depth *(a/h)* and Fracture toughness, this could lead to infinite solutions to the problem. A good practice in this case is to fix the initial notch *a=h/50*.

About F_S, can be stated that as far as no steel-bar are present, the second stage is governed by the fibre-reinforcement; this value is varied until the post-peak maximum coincides between the two curves. In conclusion, the critical embedded length is varied as far as the slopes of the third stage, pull-out tails, are the same.

In Table 8 are reported the results of the Identification procedure:

Beam ID	N_w [-]	$N_{P,f}$ [-]	K_{IC} [MPa mm$^{0.5}$]	F_S [N]	w_c [mm]
S 0.5%	231.7	0.28	90	100	2.5
S 1.0%	730	0.83	40	65	3.5
S 2.0%	938.4	0.89	40	35	4.5
AVERAGE:	-	-	56.7	66.7	3.5

Table 8: Identification procedure of Yoo et al.

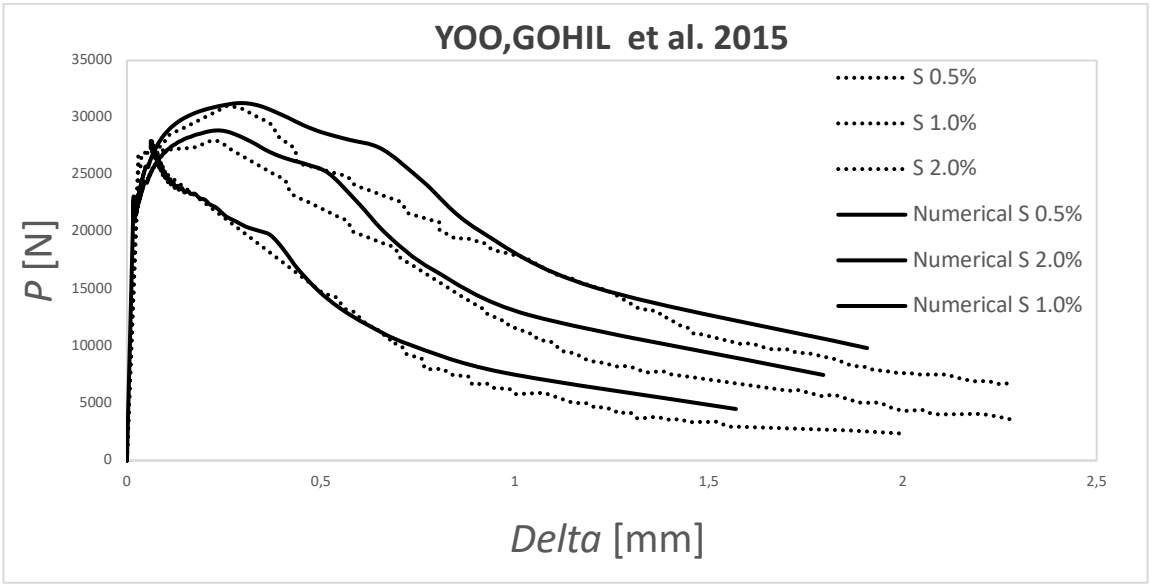

Figure 7: Yoo et al. curves (2015).

The results show a quasi-complete adherence to the experimental curves.

The other scientific paper under analysis is Bencardino [12], it is about the post-cracking behavior of High Performance Fibre Reinforced Concrete (HPFRC), aiming to test under 3-PBT and 4-PBT prismatic specimens by varying the fibre content contained in the matrix, and catching the effects of different loading condition.

The beam ID is defined as: DS stands for Dramix Steel fibres and 1%-2% is the fibre volume fraction.

The tables reported gather all the information available in the paper and useful for the input of UBCM 2.0 about concrete matrix, steel-fibre reinforcement and the results of the identification procedure.

CONCRETE MATRIX	
Properties	
E (Young's Modulus) [MPa]	81912
K_{IC} (Fracture Toughness) [MPa mm$^{0.5}$]	40
σ_c (Cubic Compressive Strength) [MPa]	80

Table 9: Concrete Matrix properties of Bencardino.

FIBRE-REINFORCEMENT	
Properties	
Typology [-]	Hooked-End
d_f (fibre diameter) [mm]	0.625
l_f (fibre length) [mm]	50
λ_f (aspect ratio) [-]	80
F_S (Pull-out force) [N]	100
w_c (Critical embedded length) [mm]	12.5

Table 10: Fibre reinforcement properties of Bencardino.

Beam ID	N_w [-]	$N_{P,f}$ [-]	K_{IC} [MPa mm$^{0.5}$]	F_S [N]	w_c [mm]
DS 1%	3.34	1.2	30	90	10
DS 2.0%	3.34	2.26	30	85	10
AVERAGE:	-	-	30.0	87.5	10.0

Table 11: Identification procedure of Bencardino.

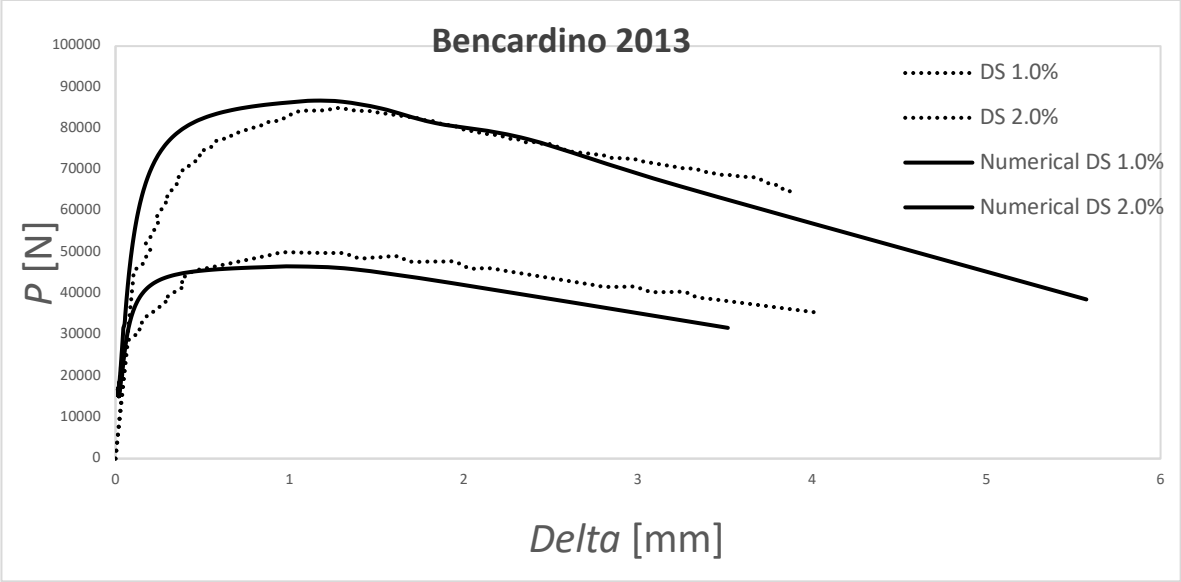

Figure 8: Bencardino curves (2013).

1.4 Model performances on PC and FRC

The last step consists into evaluate the performances of the code in terms of time of computation; the two input variables affecting that are the numerical number of fibres and the maximum iterations before convergence. This paragraph has the aim to fine tuning these two latter variables.

The curves to be represented are the four PC and FRC beams: PC40, FRC40-0.1, FRC40-0.4, FRC40-0.8; each one of that is computed for 4 values of numerical number of fibres m: 10-40-100-specimen own value of theoretical number of fibres. Then each of the 16 cases is tested for several values of maximum iterations: 10-15-30-50-100. It will be studied the relationship between the two values, to find correct indications for the final user of the code and a particular attention is put on their influence on the computation time.

What emerges from the study is that in the case of PC40, as far as no fibres are present, the variation of the maximum iteration doesn't affect the numerical solution because all the curves coincide.

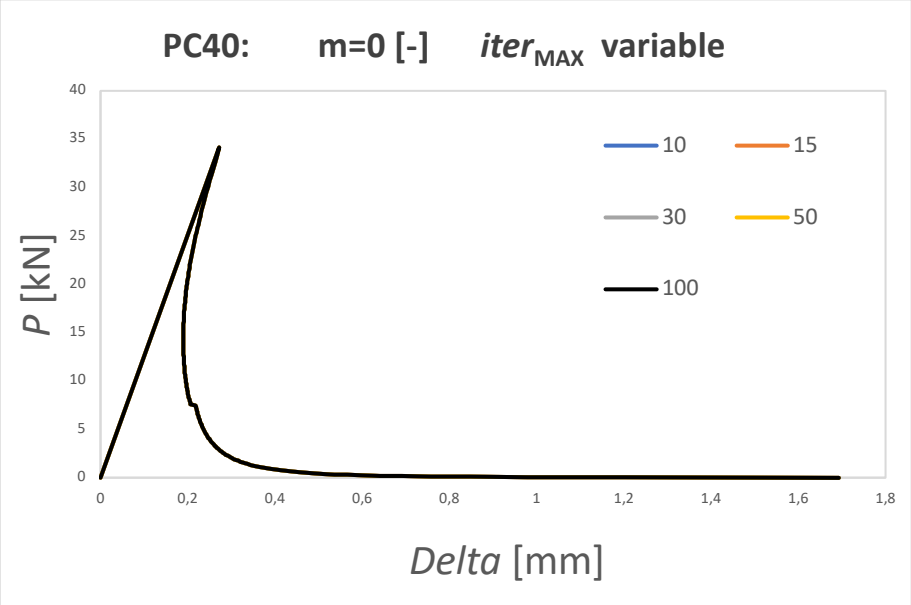

Figure 9: PC40 plotted for different maximum iterations values.

Beam ID	*m* [-]	$iter_{MAX}$ [-]	time of execution [s]
PC40	0	10	19.67
PC40	0	15	19.66
PC40	0	30	19.68
PC40	0	50	19.78
PC40	0	100	19.93

Table 12: PC40 performance parameters.

It turns out that the number of iterations is responsible of only the decimal part of the execution time, this will be confirmed as well by other beams.

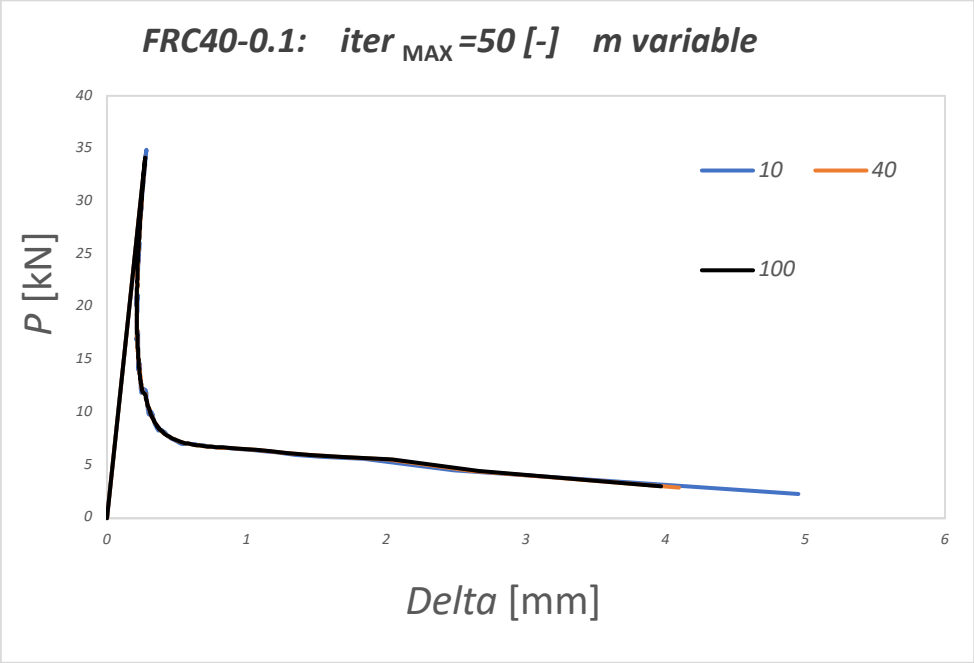

Figure 10: FRC40-0.1 plotted for different m values.

Beam ID	*m* [-]	$iter_{MAX}$ [-]	time of execution [s]
FRC40-0.1	10	10	22.27
FRC40-0.1	10	15	22.15
FRC40-0.1	10	30	22.23
FRC40-0.1	10	50	22.22
FRC40-0.1	10	100	22.32
FRC40-0.1	40	10	36.00
FRC40-0.1	40	15	35.79
FRC40-0.1	40	30	35.96
FRC40-0.1	40	50	35.82
FRC40-0.1	40	100	36.04
FRC40-0.1	100	10	106.28
FRC40-0.1	100	15	108.77
FRC40-0.1	100	30	106.88
FRC40-0.1	100	50	108.16
FRC40-0.1	100	100	107.00

Table 13: FRC40-0.8 performance parameters.

From the above results comes the confirmation of what said above: the choose of maximum iteration before convergence is only influencing the decimal part of the execution time; on the contrary, the number of numerical fibres affects the most the amount of time needed for the computation, therefore it should be properly managed.

As it's observable in Figure 10 , *m* changes the shape of the curves. The plot for 10 fibres presents higher peak and an elongated tail. As the number of fibres is increased the value of the peak remain constant and the tail shrinks to a deflection value. This could be interpreted as numerical stabilization, therefore higher value than 10 are numerically more precise. The exact trade-off in between execution time minimization and numerical precision could be *m*=40, since with *m*=100 the computation time is more than the double and the precision is almost equivalent; despite this, in the former sub-chapter the curves were plotted with higher value of numerical number of fibres, for the sake of precision in the prediction of the experiments.

Eventually, is reported the case of FRC40-0.8 for completeness, confirming what has just being said. The maximum iteration is always on safe side when approaches 100.

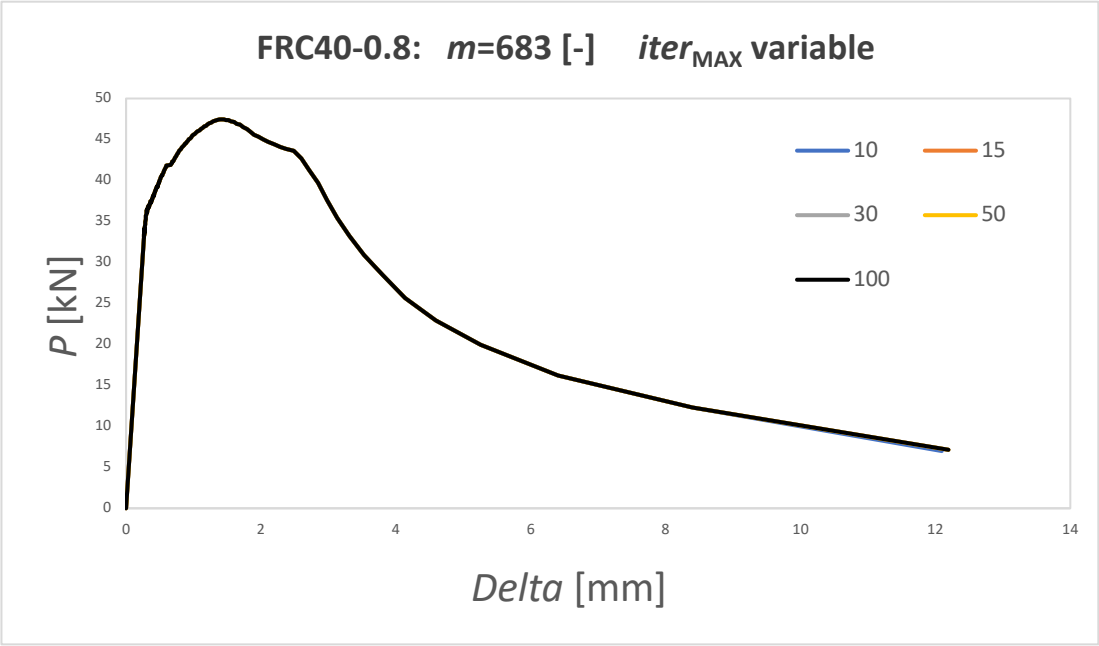

Figure 11:FRC80-0.8 plotted for different maximum iterations values.

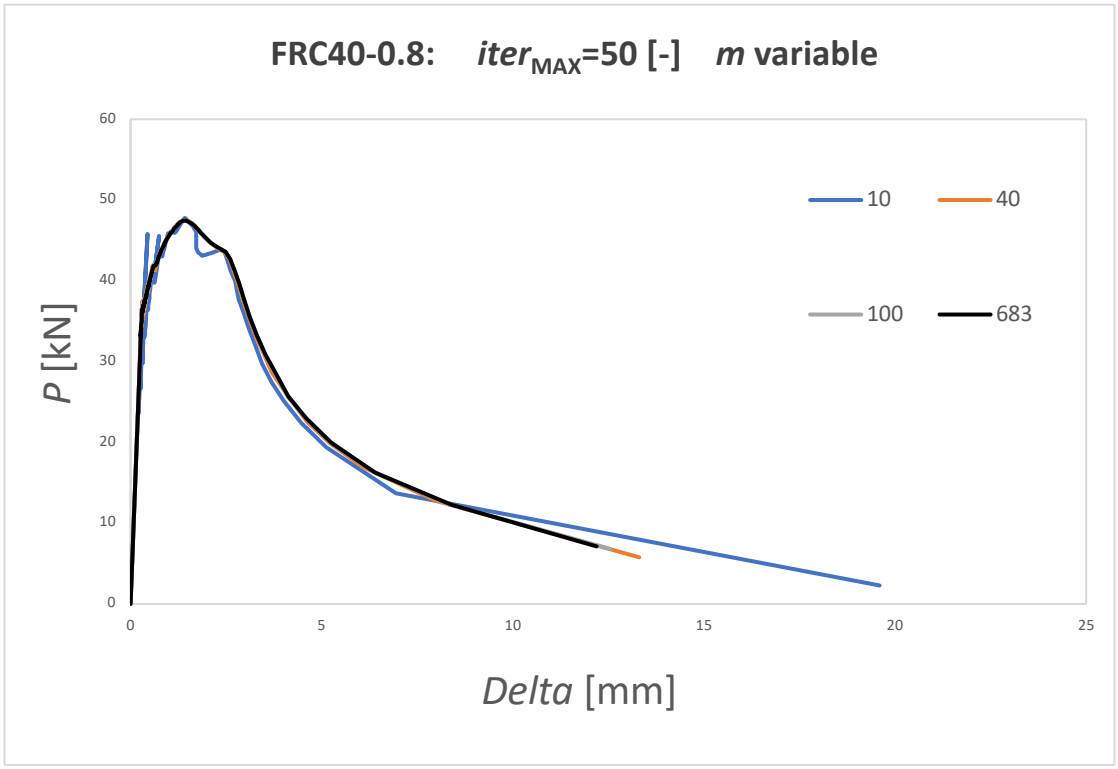

Figure 12:FRC80-0.8 plotted for different m values.

2. A Fracture mechanics approach to Tension stiffening

The second chapter of this Master Thesis deals with the relationship between the steel reinforcement bar and the adjacent concrete cover; the bi-phase response of the system is characterized by a phenomenon called *Tension Stiffening*. After a detailed literature review, a different approach to the problem, accounting for not only local interaction, is explained. A new constitutive law is introduced to model the steel-bar reinforcement, in the framework of UBCM 2.0, to account for Fibre reinforcement content, steel-bar percentage and slenderness ratio of the beam to give a more comprehensive solution. It turns out that the hypothesis yields to good fitting for Hybrid Reinforced Beam (HRC) and as well smooth results for simply Reinforced Concrete (RC) beams. Eventually, the performances of UBCM 2.0 for HRC and RC beams will be analyzed.

2.1 A literature review on Tension Stiffening

The single steel-bar subjected to tensile action will exhibit a linear elastic behavior up to the yielding displacement and then a plastic plateau; if it is coupled to a tight concrete cover, it would react differently: a first branch with greater slope, i.e., with higher Young's modulus, and then a second stage with a stiffening ascending branch. Therefore, the elastic stage in the bi-phase system will be substituted by a hardening branch, called Tension Stiffening. Historically, a first attempt to model the perfect bond relationship is by Nilson et al. [13], in the framework of finite element analysis (FEM).

Nowadays, this phenomenon is well known by technologist scholars, and it is also present in regulation; the fib Model Code [14] propose a mathematical model to account for the bond-slip between the steel and concrete, a constitutive law bond resistance versus slippage displacement. Stramandinoli et al. [15] proposes a model for nonlinear analysis of reinforced concrete

members, the concrete behaves linear elastically up to its tensile strength, in the post-cracking stage an exponential decay curve is considered until the yielding of steel takes place. The main influence over the phenomenon is addressed to the reinforcement ratio and the steel-to-concrete modular ratio, inspired by CEB model [16]. Other great achievements come from Torres et al.[17] in modeling under serviceability conditions, the instantaneous and time dependent cracking flexural behavior of RC and Prestressed concrete members, several types of loading conditions are taken into account; the solution has the aim to be straightforward and easily implemented in global algorithms.

Recent studies, introduce in the reasoning HRC and the effects of the fibres in the matrix over the tangential stress, Ding et al. [18] studied the crack arresting behavior of fibres in improving the ability of bars to withstand corrosion in aggressive environment. Glass Fibre Reinforced Polymer (GFRP), with general lower bound effect, can improve this latter if short reinforcements are present in the specimen. Chao et al. [19] proposes local bond stress-slip model for reinforcing bars and prestressing strands embedded in High Performance Fibre-Reinforced Cement Composites (HPFRCC), this leads the scientists to evaluate an effective upper bound for the shear stresses acting on the contact surface of steel and concrete, with fibres ling on it. Furthermore, Hameed et al. [20], analyzes the contribution of different fibre volume content on the stress-slip relationship at the column-beam joint, performing local pull-out tests.

However, most of the studies regard a local modelling, such as Soranakom et al. [21] which propose a “Finite difference tension stiffening model”, by chunking a 1D bar into many infinitesimal rectilinear pieces, each one giving its own contribution and connected ideally with springs to the composite matrix. A more comprehensive approach is furnished by Fantilli et al. [22], proposing a “multi-scale tension stiffening approach” to evaluate the

minimum reinforcement of HRC members; observing the phenomenon at the scale of the beam and of the surface of interaction.

2.2 The new Constitutive Law

From papers present in literature comes out that more likely is considered the local behavior of the steel-bar to model the Constitutive Law of this latter element and the bond stress versus slippage displacement relationship; nevertheless, this assumption applied to the framework of UBCM shows bad results in catching the actual experimental curves of HRC an RC. The UBCM used to describe the force versus crack opening displacement relationship of the steel-bar with the Ramberg-Osgood Law showed here below.

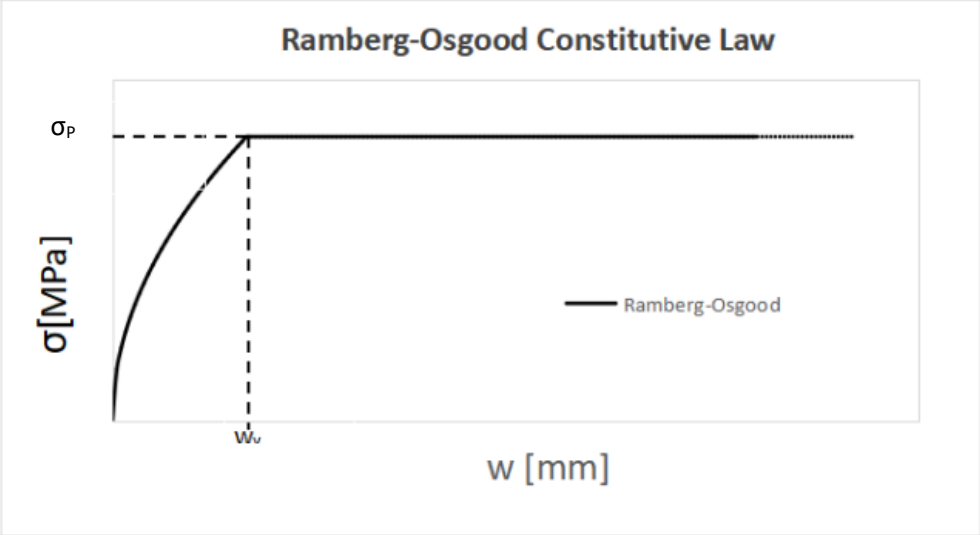

Figure 13: UBCM Ramberg-Osgood Constitutive Law.

The curve shows a first hardening branch up to w_y, i.e., Yielding Crack Opening Displacement, and a perfectly plastic behavior to infinite. The equation describing the relationship is the following:

$$\begin{cases} \sigma(w) = \sigma_P \left(\frac{w}{w_y}\right)^n & if\ w \le w_y \\ \sigma(w) = \sigma_P & else \end{cases} \qquad \text{(Eq. 2.1)}$$

Where *n* is the so called Ramberg-Osgood exponent, which is constant and equal to 0,5.

This hypothesis yields to good results in catching the first elastic stage of both HRC and RC beams, as well as catching the third softening stage, just after the Post-cracking; despite that, it fails in the evaluation of pre-peak stage, it means the stage at which tension stiffening acts, and bad evaluate peak load too. Many experimental curves have been observed, and after careful analysis is noted that the issue could be connected to the constant value of w_y. The yielding crack opening displacement is calculated with the formula furnished by Ruiz et al. [23]:

$$w_y = \frac{\sigma_P^2 \, \Phi}{4 \, E_s \tau_m} \qquad \text{(Eq. 2.2)}$$

Where:

- σ_P : is the yielding strength of the steel-bar [MPa]

- Φ: is the steel-bar diameter [mm]

- E_s: is the steel-bar Young modulus [MPa]

- τ_m: is the mean shear stress acting on the concrete contact surface [MPa]

(Eq.2.2) accounts only for the friction arising between concrete and steel during flexure, providing only local insights about the phenomenon.

In the UBCM 2.0 framework is introduced a new constitutive law, accounting for the global behavior of the structure; by means specific quantities: Slenderness ratio λ, gathering somehow the dimension of the specimen, the fibre volume fraction V_f and the reinforcement ratio ρ. The influence of the above-mentioned quantities is contained in a coefficient called "*n* of Tension Stiffening", being a nonlinear function of these quantities:

$$n = f(\lambda ; V_f ; \rho) \qquad \text{(Eq. 2.3)}$$

The n-value is directly manipulating w_y, depending only on local phenomena, in this way:

$$w_{y,real} = \frac{w_y}{n} \qquad \text{(Eq. 2.4)}$$

In an easy way, can be said that if n is greater than 1, the value of the real yielding crack opening displacement would decrease; on the contrary, if $0 < n \leq 1$ $w_{y,real}$ would increase. This concept is used to rework (Eq. 2.1): an exponential term is added to guarantee an asymptotic behavior tending to the yielding strength of the steel-bar, the n of tension stiffening is considered as well:

$$\sigma(w) = \sigma_P \left[1 - e^{-n\left(w/w_y\right)} \right] \qquad (\text{Eq. } 2.5)$$

Then in the Figure 14 is showed (Eq. 2.5) plotted for many values of *n*:

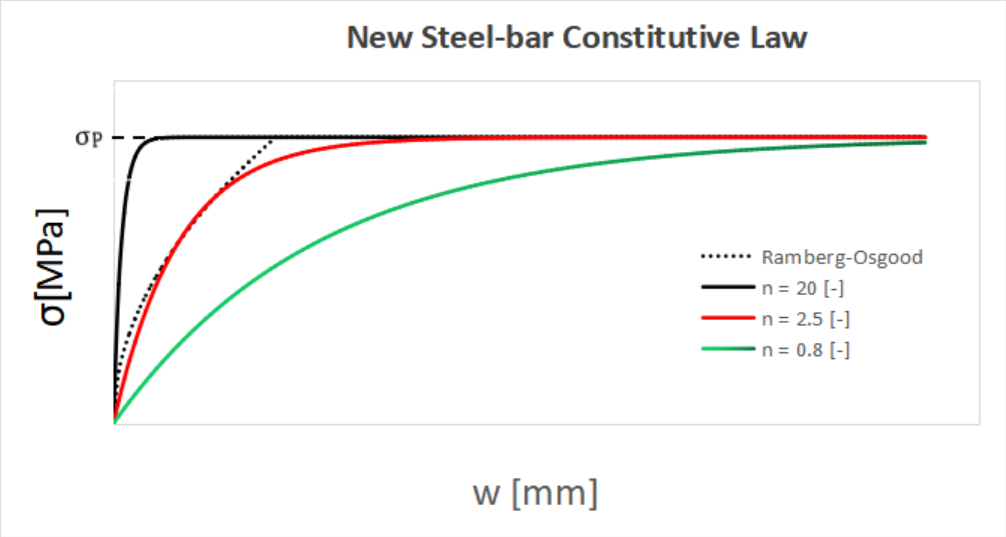

Figure 14: New Steel-bar Constitutive Law for UBCM 2.0.

From a graphical point of view, it can be noted that n controls the slope of the hardening branch; this is the mathematical trick that enable the correct representation of the HRC and RC curves.

2.3 Identification of "*n* of Tension Stiffening"

As far as the function describing n is unknown, large amount of data should be collected by identifying existing curves in literature. The studies analyzed consider 4-PBT and 3-PBT of RC and HRC beams, the results could be expressed in load

versus mid-span deflection or bending moment versus mid-span deflection. The general identification procedure for HRC involves five quantities, the former three are the same of the FRC beams, in addiction the steel-bar yielding strength and n should be identified:

- K_{IC}: Fracture toughness, regarding the concrete matrix.

- F_s: Pull-out force of the single fibre, sometimes expressed as $\bar{\sigma}_s$[MPa] i.e. slippage strength of the fibre.

- w_c: Critical embedded length of the fibre.

- σ_P: Yielding strength of steel-bar

- *n*: *n* of Tension Stiffening.

The retrieval of the starting triplex has already been explained in the paragraph 1.3.2; regarding the latter two: σ_P should be changed by catching the level of the plastic plateau; eventually, *n* is correctly evaluated when the pre-peak shape of the numerical curve approximates the better the experimental one.

The procedure just described is performed for a number of 28 curves, coming from several authors; the data-frame extracted will be analyzed afterward in this chapter. Now, to clarify the research work performed, some example curves are plotted.

The first paper under identification is Holschemacher et al. [24], which investigates the effect of steel fibres in mechanical properties of HRC and RC beams; it is interesting for the objective of this Master Thesis because, the steel-bar reinforcement ratio and the size are maintained constant by varying the fibre volume fraction. The beam ID is composed in this way: B indicates the beams having ρ=0.26%; the number 20-40-60 indicates the fibre volume fraction V_f measured in [kg/m$^{3]}$. The prismatic elements have dimensions *t=15 cm, h=15 cm* and *S=60 cm*; as far as the beams are unnotched the initial crack depth is put *a=h/50,* to let the simulation being a good approximation of the reality.

Here below are reported tables gathering the data of the matrix and reinforcements retrieved from the original paper:

CONCRETE MATRIX

Properties	
f_{cm} (Compression Strength) [MPa]	86

Table 14: Matric properties of Holschemacher et al.

Properties	
Typology [-]	Hooked-End
l_f (fibre length) [mm]	50
f_u (fibre tensile strength) [MPa]	1100-1900

Table 15: Fibre reinforcement properties of Holschemacher et al.

STEEL-BAR REINFORCEMENT

Properties	
σ_P (bar yield strength) [MPa]	500

Table 16: Steel-bar reinforcement properties for Holschemacher et al.

Here below are summarized the results of the identification:

Beam ID	Type [-]	K_{IC} [MPa mm$^{0.5}$]	σ_P [MPa]	F_s[N]	w_c[mm]	n [-]
B-0	RC	64	800	35	10	60
B-20	HRC	64	800	35	10	5
B-40	HRC	64	800	35	10	1.3
B-60	HRC	64	800	35	10	0.8

Table 17: Identification for Holschemacher.

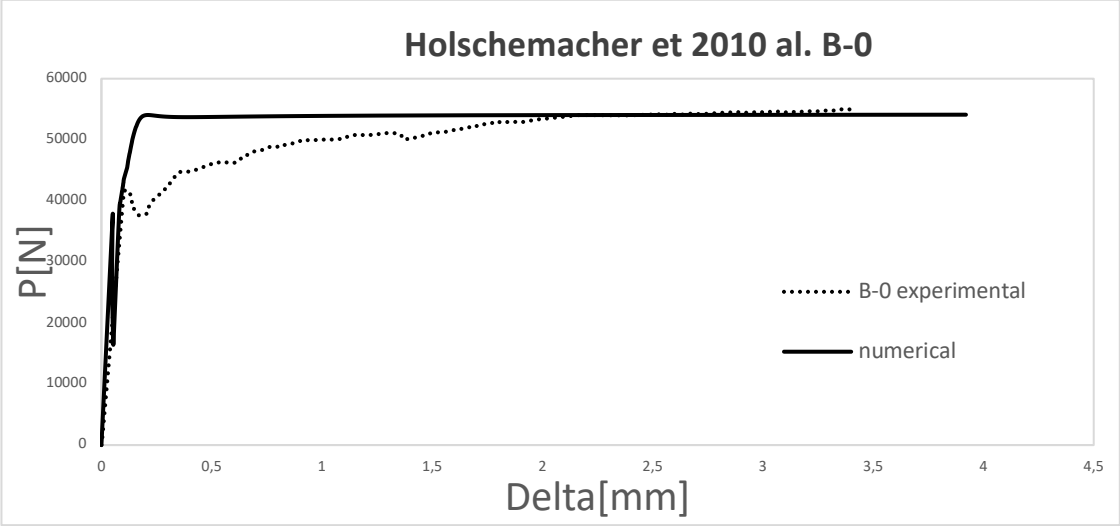

Figure 15: Holschemacher B-0 curve.

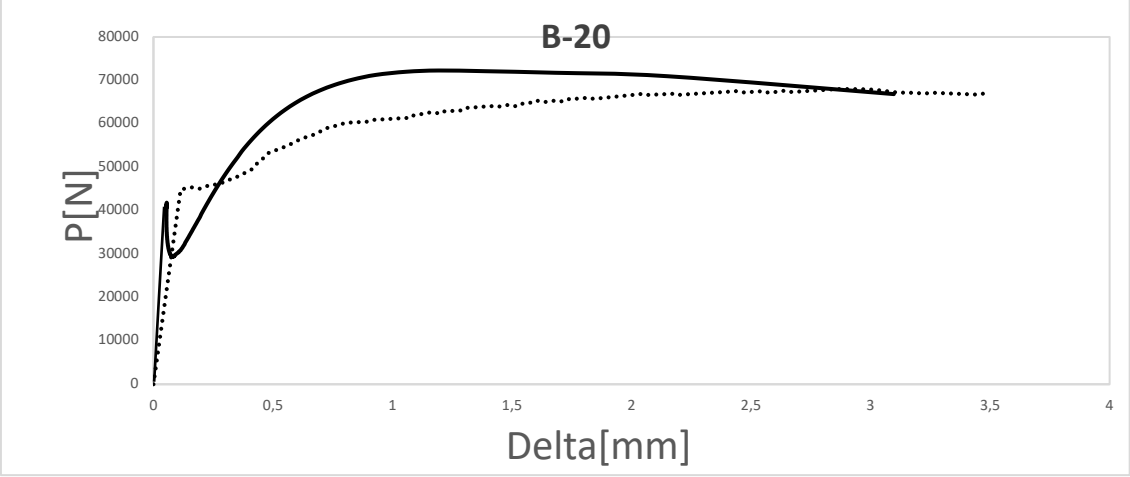

Figure 16: Holschemacher B-20 curve.

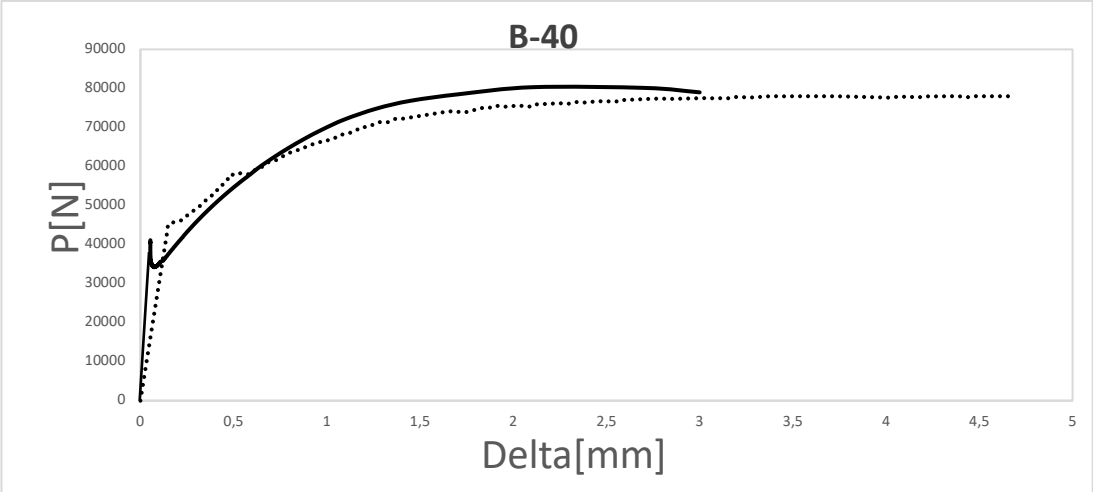

Figure 17: Holschemacher B-40 curve.

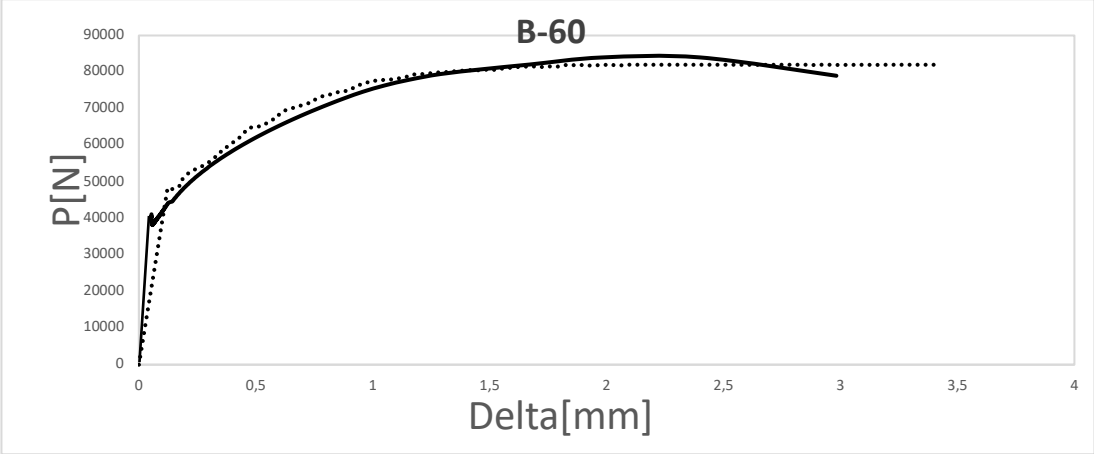

Figure 18: Holschemacher B-60 curve.

The second scientific paper to be presented is by Oliveira [25], which want to prove the positive factors in reducing the amount of steel-bar reinforcement in RC with the addiction of fibre, changing also the strength grade of concrete. It is worthy to note that, as in the previous case, the steel-bar reinforcement ratio is maintained constant by varying the fibre content; the beam IDs are defined as FC30-FC60 indicating the grade of concrete, F00-F45-…-F90 states the fibre volume fraction V_f in [kg/m^3]. The case of FC30F00 has higher tensile reinforcement ρ=0.91%, whereas the other cases present ρ=0.39%; in both the situations is present the upper edge reinforcement in the minimum percentage provided by regulations.

The dimensions of the beams tested under 4-PBT are *t*=15 cm, *h=30 cm* and *S=250 cm.*

The identification is performed giving as results:

Beam ID	Type [-]	K_{IC} [MPa mm$^{0.5}$]	σ_P [MPa]	F_s [N]	w_c [mm]	*n* [-]
FC30CF00	RC	30	170	0	0	0.08
FC60CF45	HRC	30	320	35	15	0.15
FC60CF60	HRC	30	330	30	15	0.11
FC60CF75	HRC	30	330	30	15	0.10
FC60CF90	HRC	30	350	35	15	0.09

Table 15: Identification for Oliveira et al.

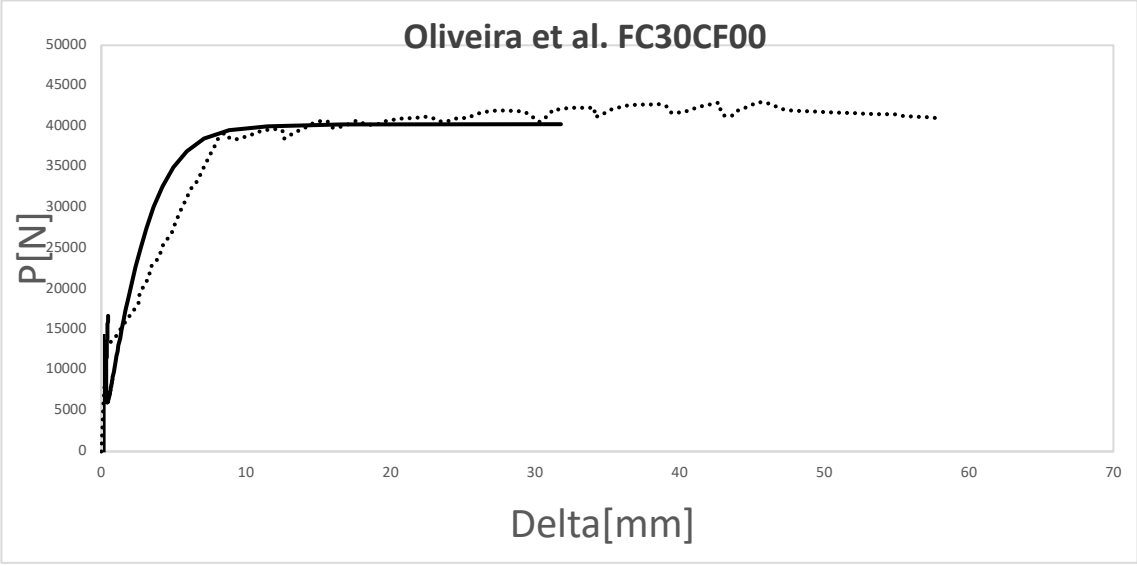

Figure 19: Oliveira FC30CF00.

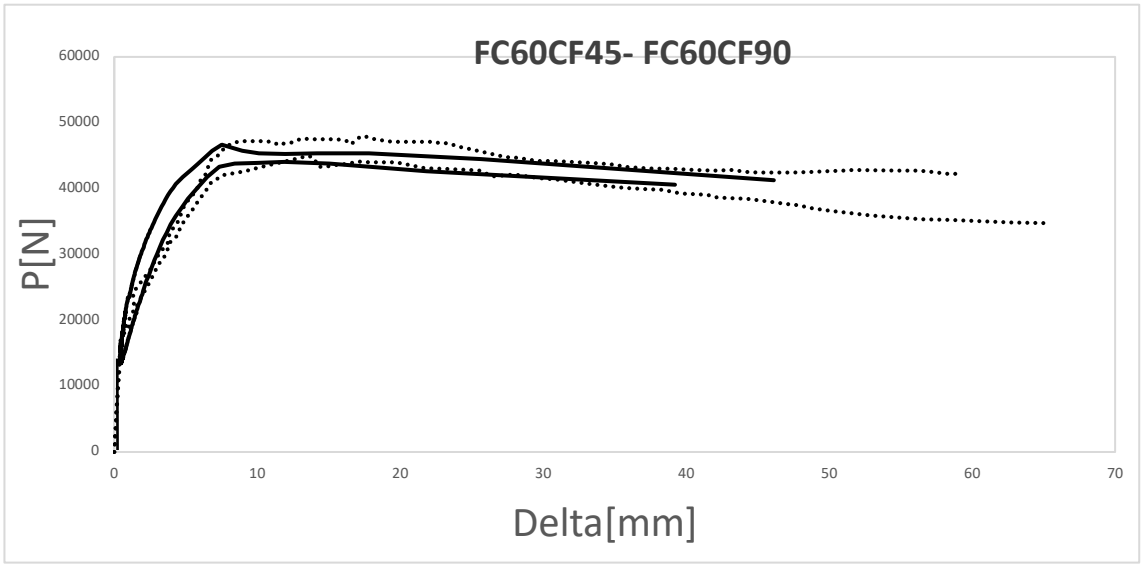

Figure 20: Oliveira FC60CF45 and FC60CF90.

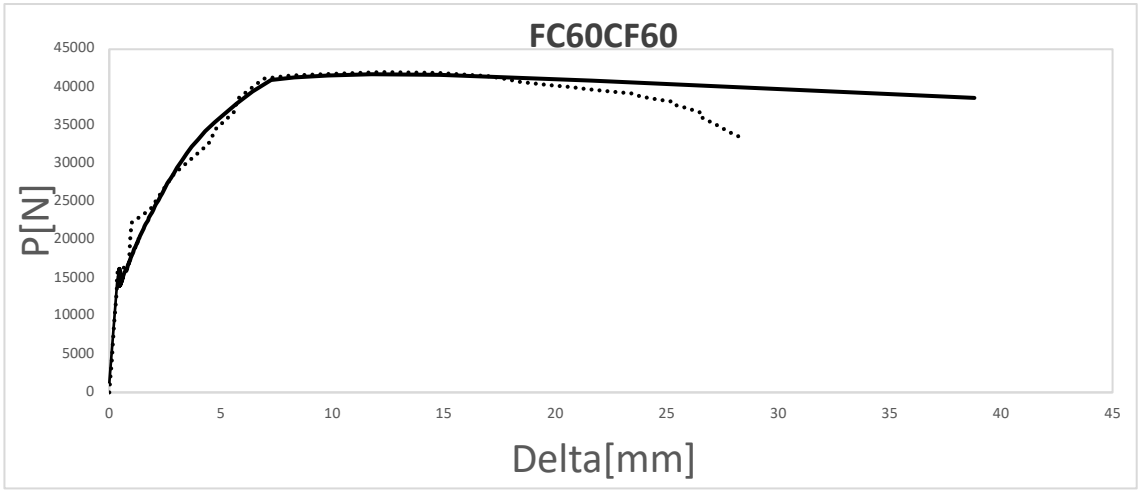

Figure 21: Oliveira FC60CF60.

Then, it is done an attempt to describe the physical meaning of *n* and its relationship with w_y. Talking about these two papers, a quite interesting trend can be caught by the results.

The case of the first Holschemacher paper is reported in the below pictures:

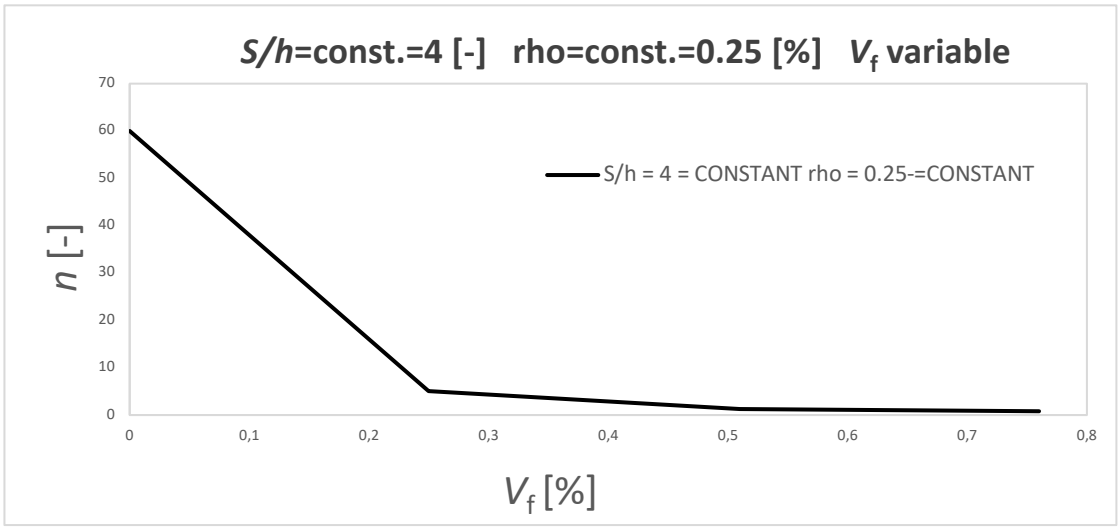

Figure 22: n trend in Holschemacher curves.

It can be noted a tri-linear monotonic decreasing behavior by varying the fibre volume fraction, considering as constant the slenderness and the steel-bar reinforcement ratio. In terms of yielding crack displacement, the trend will be:

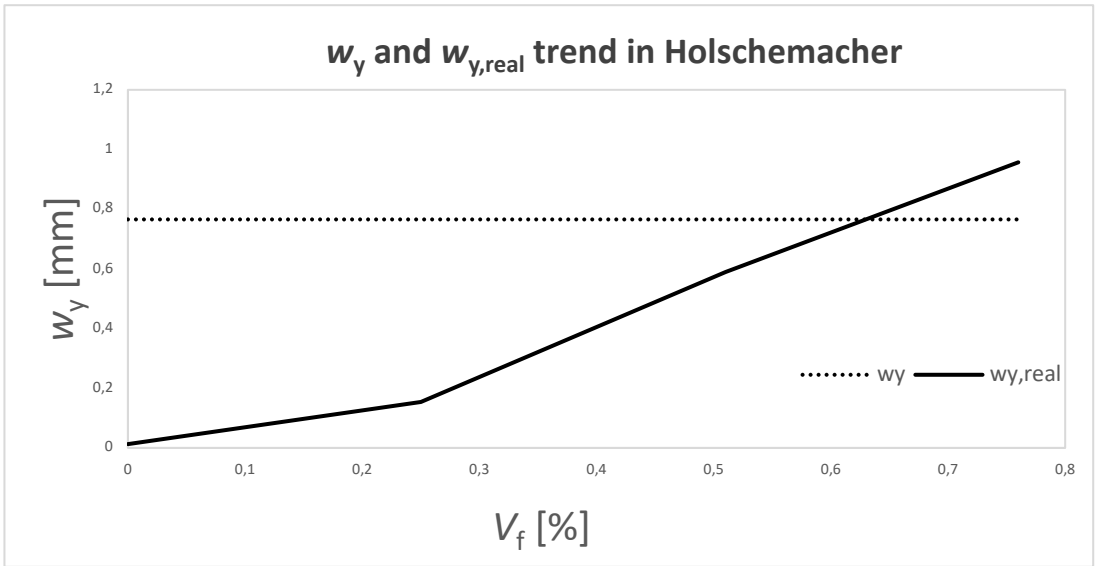

Figure 23: w_y and $w_{y,real}$ Holschemacher.

And in a tabular format:

Source name	Type	ID	V_f [%]	w_y[mm]	$w_{y,real}$ [mm]	n [-]
Hoelsmacher et al.	RC	B-0	0	0.7657	0.013	60
Hoelsmacher et al.	HRC	B-20	0.25	0.7657	0.153	5
Hoelsmacher et al.	HRC	B-40	0.51	0.7657	0.589	1.3
Hoelsmacher et al.	HRC	B-60	0.76	0.7657	0.957	0.8

Table 18: w_y and $w_{y,real}$ trend Holschemacher.

From both Figure 23 and Table 15 is understandable that w_y is not constant such as suggested by Ruiz (Eq.2.2), but in this case has a monotonic increasing trend, as the fibre content is increased. This could be explained physically, by the fact that fibres are acting on the contact surface between concrete and steel-bar, enhancing the bonding between the two phases; therefore, the yielding point is 0.013 mm in the case of B-0 RC beam, and it is increase up to 0.957 mm in the case of the highest fibre reinforced HRC. At the end of the reasoning, it can be stated that bar is yielding at higher displacement value in HRC and yielding at lower value if no fibre are present as in the RC beam. Similar trend is observed in the case of the second Oliveira paper:

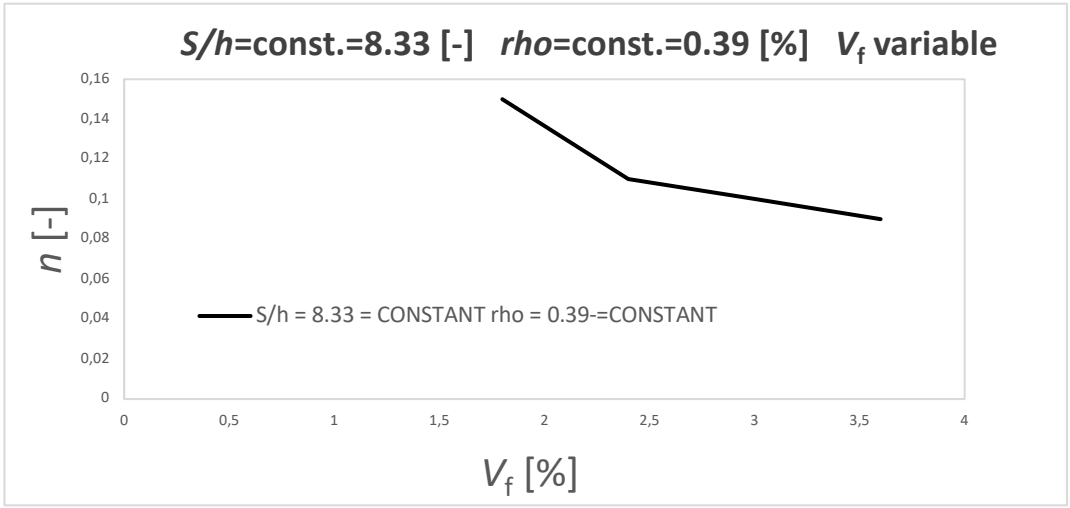

Figure 24: n trend of Oliveira.

As well as Holschemacher the observed trend is monotonic decreasing with fibre content increasing.

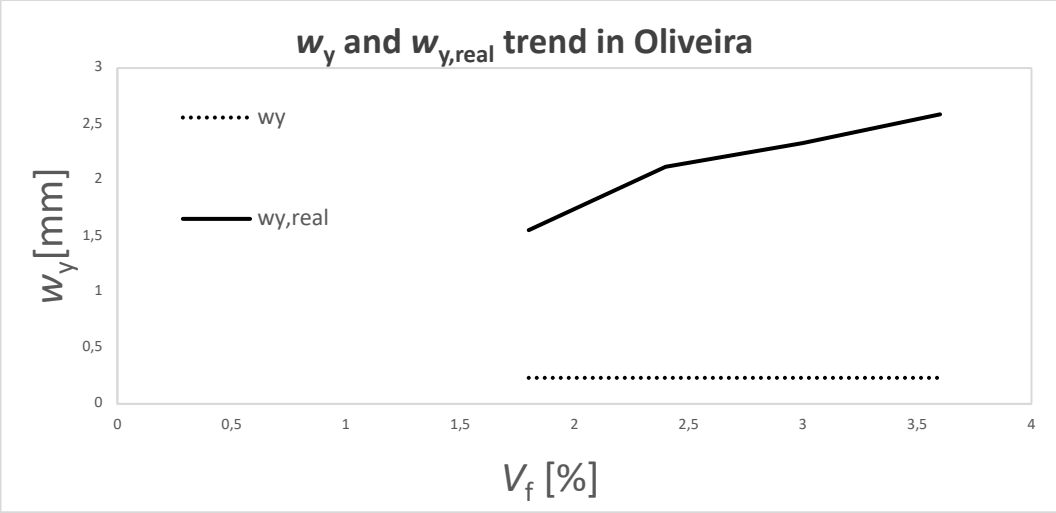

Figure 25: wy and wy,real trend in Oliveira.

Source name	Type	ID	V_f [%]	w_y[mm]	$w_{y,real}$ [mm]	n [-]
Oliveira et al.	RC	FC30CF00	0	0.3695	0.462	0.8
Oliveira et al.	HRC	FC60CF45	1.8	0.2328	1.552	0.15
Oliveira et al.	HRC	FC30CF00	2.4	0.2328	2.116	0.11
Oliveira et al.	HRC	FC30CF00	3	0.2328	2.328	0.1
Oliveira et al.	HRC	FC30CF00	3.6	0.2328	2.587	0.09

Table 19: w_y and $w_{y,real}$ trend in Oliveira.

In this case the RC beam is not represented as far as it presents different reinforcement ratio; however, the behavior is the same as the first paper. The values of $w_{y,real}$ are actually much higher than Holschemacher curves, this is due to the fact that the scale and the materials differ a lot.

What is highlighted again is the fact that steel-bar, maintaining constant the steel-bar percentage and the slenderness, as the amount of fibres increases is yielding at higher displacements, it means that the crack should spread more to excite the tensile reinforcement.

Lastly, is performed an assessment of the good design of all the 28 prismatic specimens analyzed, in terms of minimum amount of steel-bar and fibre reinforcement. If not well designed, the fact could lead to uncertain results and therefore even less precise outcomes in the parametric analysis. To verify that all the beams are represented in terms of N_P, steel-bar reinforcement brittleness number and $N_{P,f}$, fibre-reinforcement brittleness number. The plot in the graph of these 28 points shows that all the curves are belonging to the Stable region, above the Regression line in which lays critical values of the brittleness parameters.

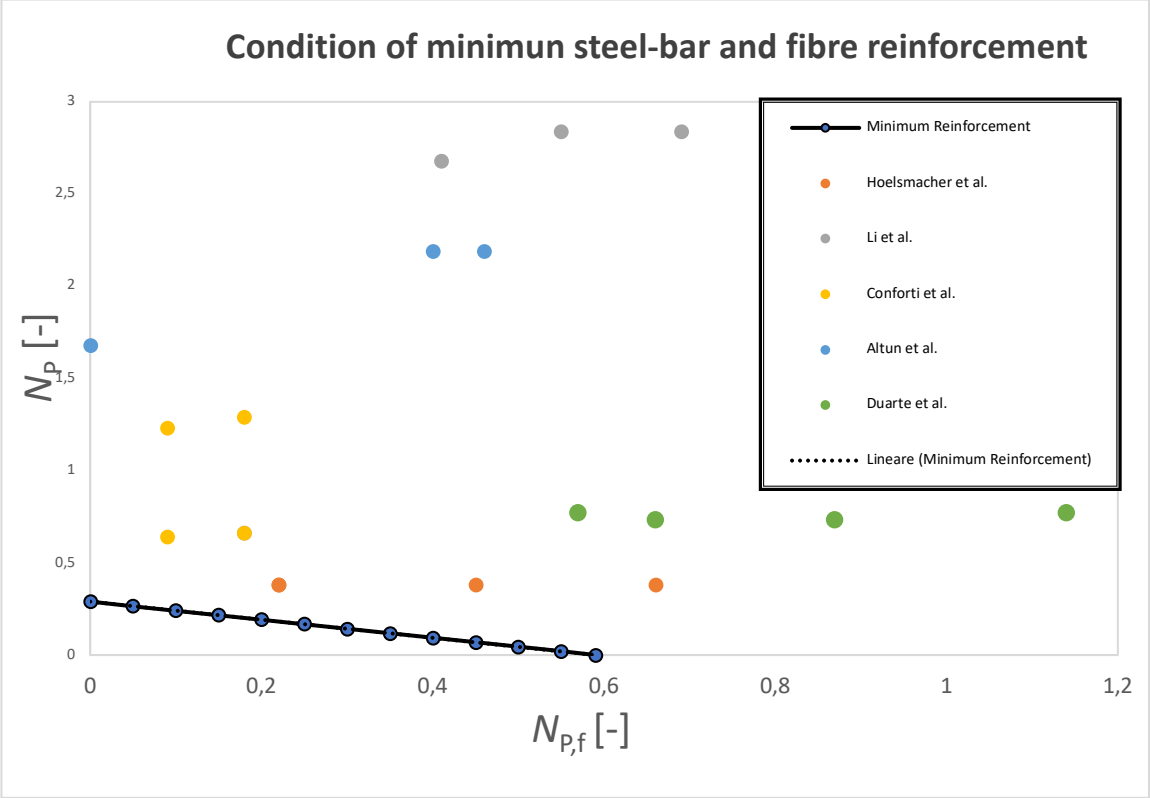

Figure 26: Condition of minimum reinforcement for experimental curves.

2.4 *n* parametric analysis with K-NN Machine Learning algorithm.

In the previous chapter is highlighted an evident trend of *n* and of the yielding crack opening displacement, also explained by a logical physical meaning; despite this fact, the analysis turns out to be hard. As a matter of fact, changing the specimen's dimension and the amount of reinforcement the behaviors showed are not trivial; also, owing to the scarcity and heterogeneity of data present in literature.

For instance, in the below figure is represented n trend for two different cases, obtained by maintaining constant the slenderness and the fibre volume content, with steel percentage variable:

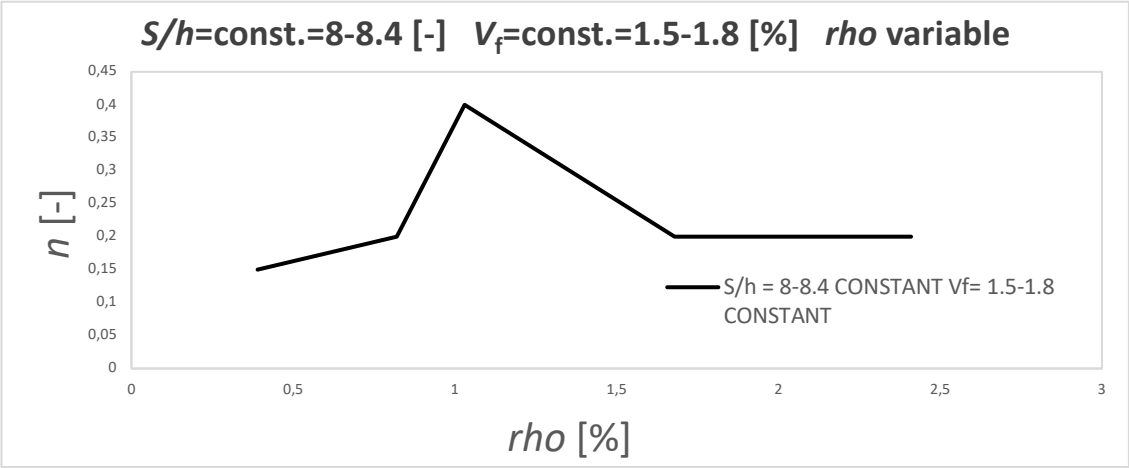

Figure 27: First n trend by varying rho.

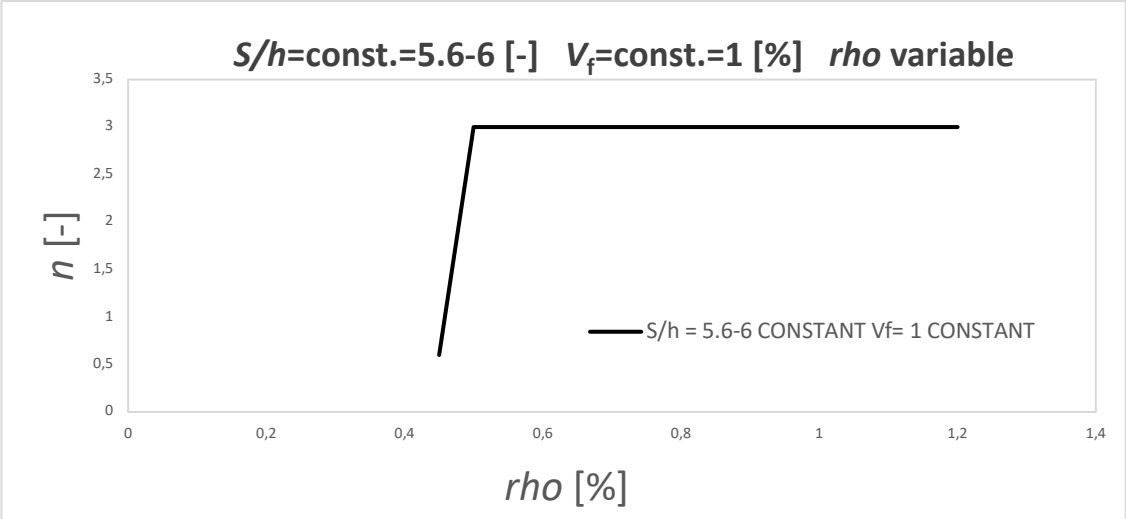

Figure 28: Second n trend by varying rho.

The situation becomes even more fuzzy by varying the slenderness of the beam, maintaining constant the reinforcement parameters.

Owing to this fact a not clear path through data can be identified; therefore, it is used a simple Machine Learning algorithm to predict *n* of Tension Stiffening for new curves, to model in a proper way new beams.

The chosen one is the *K nearest neighbors algorithm (K-NN)* [31]. Before describing the model, is useful to identify the problem in the database that should be solved by means this framework: the data-frame presents 28 rows, also called in data analysis *records*, and it have several f columns, also known as *features.* Each record defines a beam, and each f features represent indeed a characteristic of the specimen such as: height, depth, Fracture Toughness, Fibre Volume content etc. Out of the f-columns, three main characteristics are chosen to properly describe the specimen:

- λ : Slenderness ratio [-]
- V_f Fibre Volume Fraction [%]
- ρ : Steel-bar reinforcement ratio [%]

These quantities have been chosen because practically is observed a change in *n* as one of the three is varied. Regarding the unit of measure of the variables, is chosen the one that let data being homogeneous, therefore not much distant in the mathematical 3-D space in which beams are conceptually represented. Furthermore, the number of columns selected is good, because increasing the number of axes in the mathematical space (for instance a beam identified by 6 features, will be represented in a 6-D space) the K-NN model would suffer by the so-called *curse of dimensionality*, decreasing its precision in finding meaningful neighbors. Eventually, at each row of the database is connected a value of n, called *label* in the context of data analysis.

The problem is defined as *Regression,* because the value that should be predicted is a real value, in this case *n*.

The K-NN is very versatility and easy to implement, in the analyzed case is a great decision because few records are present, and the number of influencing features is low.

Each beam, in this context, is represented in 3-D space in which: x-axis represents the slenderness, y-axis represents the fibre volume fraction and the latter z-axis define its steel-bar percentage; each one of this point has a label containing the real value of *n* identified. Imaging that is required to identify the *n* of Tension Stiffening of a new beam, introducing the known value of the three characteristics of the new specimen, the predicted n-value will be the average of the labels of the K nearest points in this mathematical space. K is a model parameter that should be properly tuned.

This is the Dataset obtained by means identification procedure of 28 curves in literature:

rho [%]	V_f [%]	*S/h* [-]	*n* [-]
0.76	0	11.33	0.2
0.76	0	11.33	0.2
0.81	0	11.33	0.2
0.25	0	4.00	60
0.25	0.25	4.00	5
0.25	0.51	4.00	1.3
0.25	0.76	4.00	0.8
0.82	1.5	8.40	0.2
1.68	1.5	8.40	0.2
2.41	1.5	8.40	0.2
0.5	1	5.60	3
0.5	2	5.60	3
1.2	1	5.60	3
1.2	2	5.60	3
1.03	0	8.00	0.4
1.03	0.8	8.00	0.4
1.03	1.2	8.00	0.4
1.03	1.6	8.00	0.4
1.03	2	8.00	0.4
0.45	0	6.00	0.8
0.45	1	6.00	0.6
0.45	0	6.00	0.8
0.45	1	6.00	0.6
0.91	0	8.33	0.8
0.39	1.8	8.33	0.15
0.39	2.4	8.33	0.11
0.39	3	8.33	0.1
0.39	3.6	8.33	0.09

Table 20: Dataset for K-NN algorithm.

The number of observations is quite small, the general approach to the problem is to gather the 80% of the data into a smaller set called *Train set*, useful to set up the parameters of the model; the remaining 20% is called *Test set*, by means which the accuracy of the system is calculated. In this case a *Cross validation* tool is performed to act against scarcity of data, it consists on splitting the data-frame in smaller sets, 3 folds are enough to achieve coherent results, and in a round-robin fashion one chunk is used as test set for the other two.

The fine tuning of K, number of neighbors, is analyzed by letting it vary in between 1 and 20; the correct value of K is found by minimizing the so called Mean Absolute Error:

$$\mathrm{MAE_k} = \frac{\sum_1^3 \left|\mathrm{n_{test-set}(i)} - \mathrm{n_{predicted}(i)}\right|}{3} \quad \forall \mathrm{k} = \{1,2\ldots 20\} \qquad (\mathrm{Eq.\ 2.6})$$

Therefore, being K=7 the case with the minimum MAE_k, it is selected as effective model parameter to make prediction.

The framework analyzed, despite the low amount of data present in literature, embodies a good tool to predict *n* value for the numerical curves of the large test campaign based at Shantou University.

2.5 Numerical curves

The direct prediction of the behavior of the following curves is of great importance for three main reasons: assess the UBCM 2.0, verify the correct prediction of K-NN model for *n* Tension Stiffening and to plot the curves itself, being a guideline for the test campaign.

The HRC and RC beams are 80 in total: the properties of the concrete matrix and fibre-reinforcement are the same reported in Chapter 1 (Table 1 and Table 1Table 2), the steel-bar has a yielding strength equal to 450 MPa, its diameter is varying case by case. The concrete cover is assumed to be equal to the initial notch: *c=a=h/10*. The selection about the numerical number of fibres is made in accordance to what said in Chapter 1, if theoretical number of fibres is below 100 the actual quantity is used, otherwise 100 numerical number is chosen. The beam IDs are defined in this way: RC stands for Reinforced Concrete, HRC stands for Hybrid Reinforced Concrete; the number 20,40,80,160 refer to the depth of the beam in cm; the second number is the reinforcement ratio multiplied by 100; eventually the third number is the fibre volume fraction in percentage.

The loading condition is 4-PBT, as showed in the below figure:

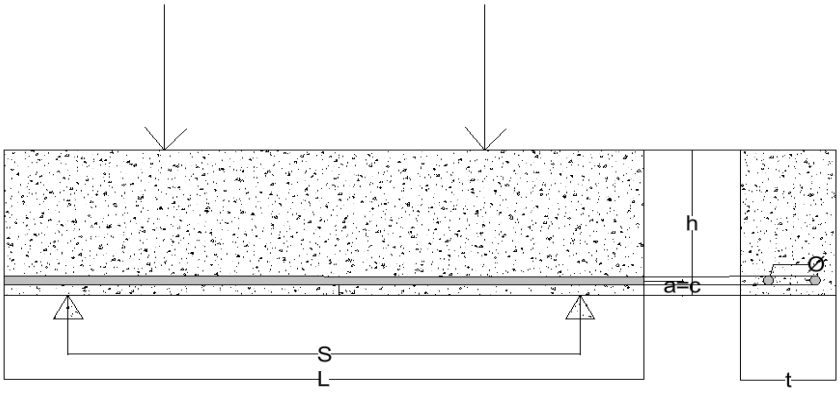

Figure 29: 4-PBT scheme.

As far as in the test campaign the slenderness ratio is constant, the steel-bar reinforcement ratio can assume 4 values and the fibre volume fraction 5, the K-NN should predict *n* of Tension Stiffening only for 20 situations:

rho [%]	V_f [%]	*S/h* [-]	*n* [-]
0.06	0	6.00	0.8
0.06	0.1	6.00	0.8
0.06	0.2	6.00	0.8
0.06	0.4	6.00	0.8
0.06	0.8	6.00	0.6
0.13	0	6.00	0.8
0.13	0.1	6.00	0.8
0.13	0.2	6.00	0.8
0.13	0.4	6.00	0.8
0.13	0.8	6.00	0.6
0.28	0	6.00	0.8
0.28	0.1	6.00	0.8
0.28	0.2	6.00	0.8
0.28	0.4	6.00	0.8
0.28	0.8	6.00	0.6
0.5	0	6.00	0.8
0.5	0.1	6.00	0.8
0.5	0.2	6.00	0.8
0.5	0.4	6.00	0.8
0.5	0.8	6.00	0.6

Table 21: n K-NN predictions.

Despite the fact the Train set is very small, the predicted values seem reliable; they represent a good starting point for new data, however, an identification procedure after the practical test is suggested. One of the main outcomes of the

test campaign could be the use of the new curves to enlarge the test set of K-NN upgrading its capability to generalize over new data.

Are there plotted all the prismatic specimen having depth equal to 80 cm:

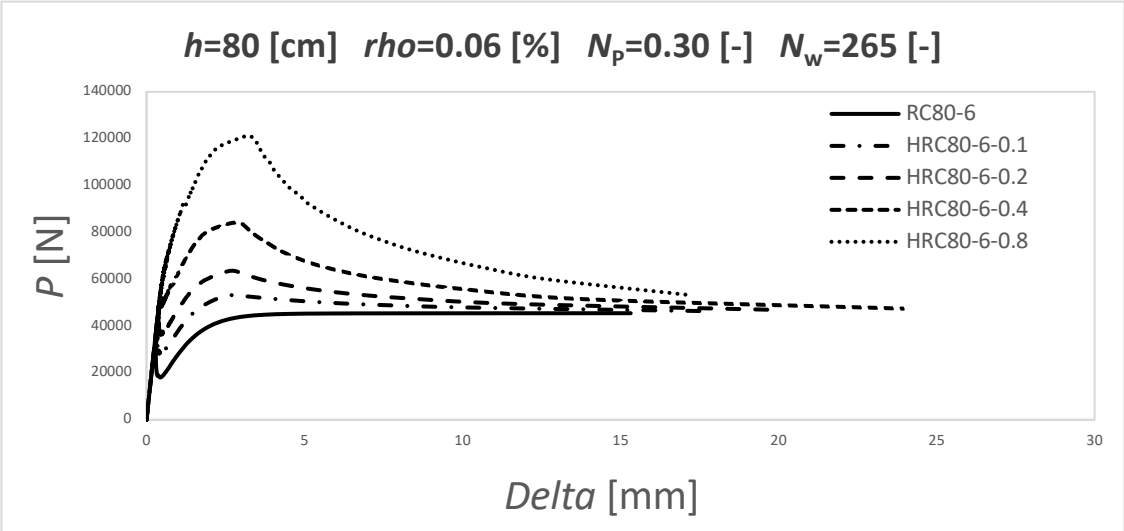

Figure 30: Numerical curves h=80cm rho=0.06%.

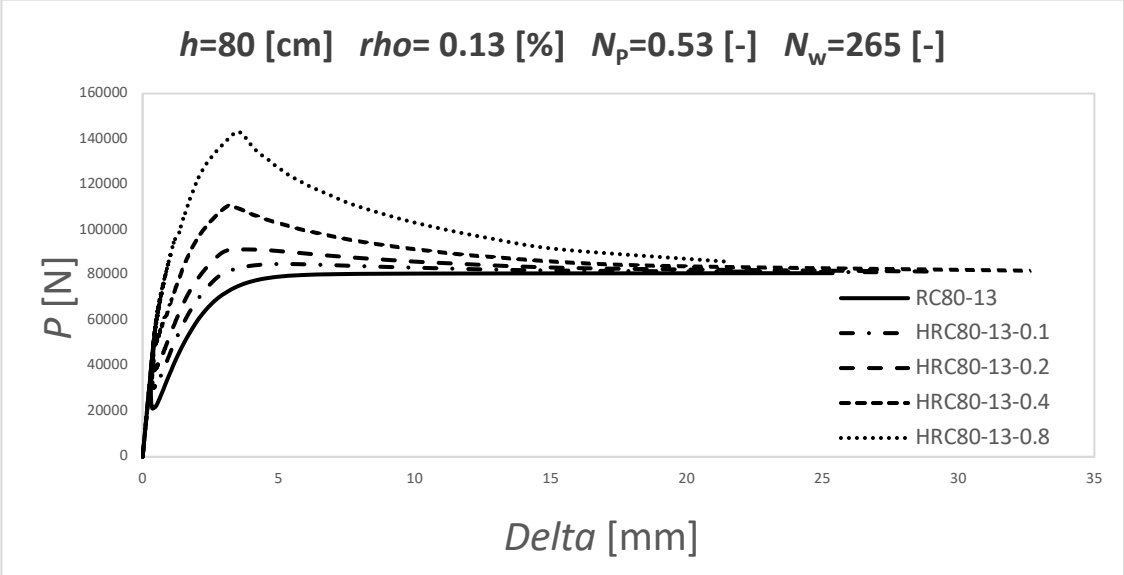

Figure 31: Numerical curves h=80 cm rho=0.13%.

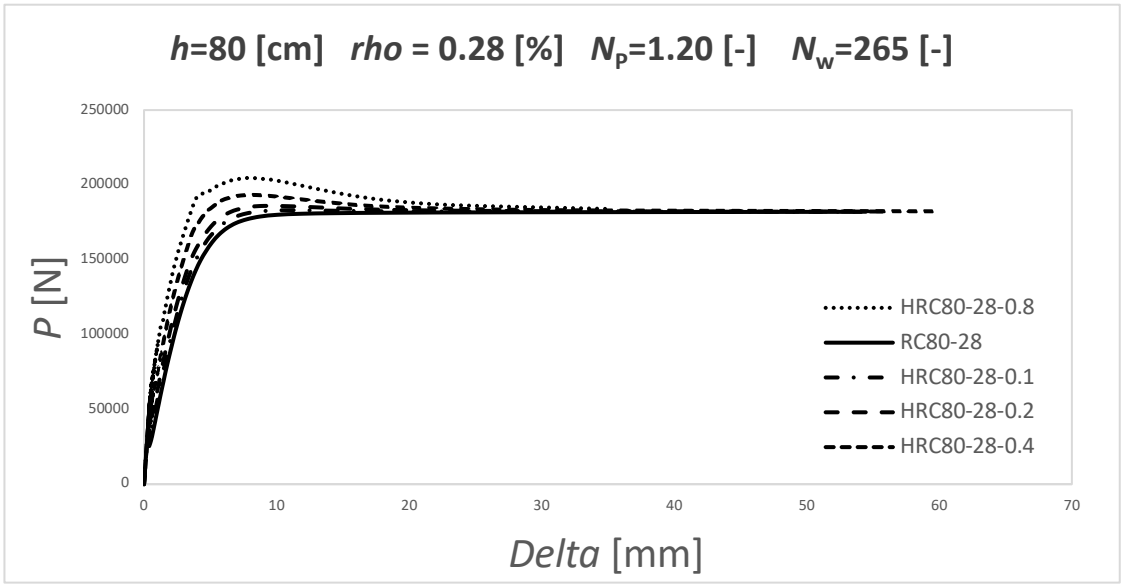

Figure 32: Numerical curves h=80cm rho=0.28%.

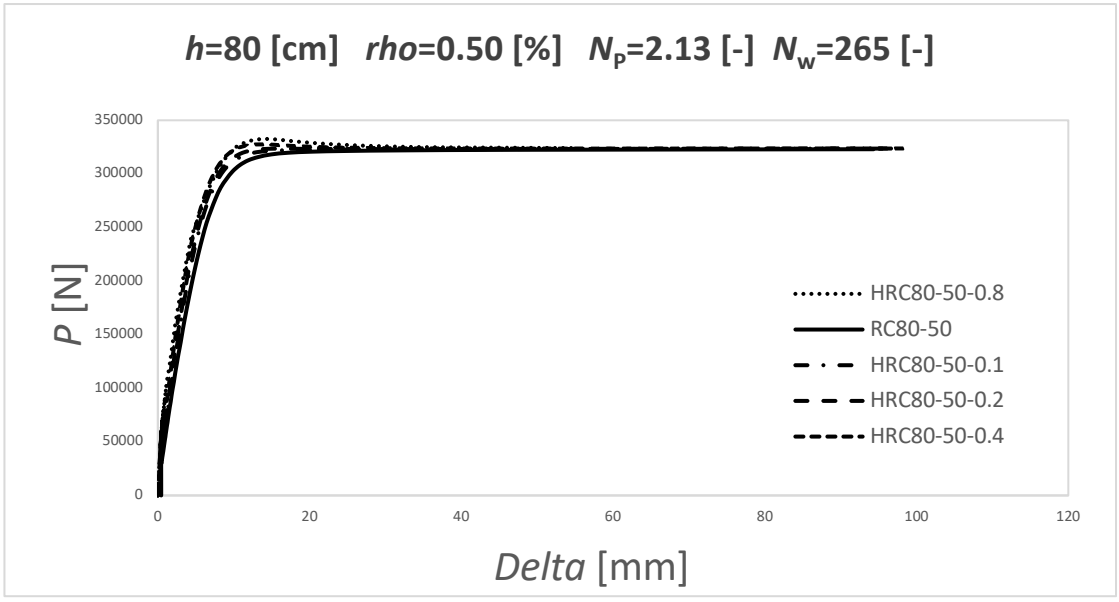

Figure 33: Numerical curves h=80cm rho=0.50%.

For HRC the following relationship is established:

$$\Pi(M_F, \Theta; K_{IC}, E; V_F, \sigma_s, w_c; \rho, \sigma_y; b, h, a) = 0 \qquad \text{(Eq. 2.7)}$$

Whit respect to FRC, the steel-bar reinforcement and the yielding strength of bar is added; as done in previous chapter: assuming $(\mathrm{K_{IC}}, \mathrm{h})$ as independent variables, the (Eq. 2.7) can be rewritten as:

$$\Pi^*\left(\frac{M_\mathrm{F}}{K_\mathrm{IC} b h^{3/2}}, \Theta\frac{E}{K_\mathrm{IC}}h^{1/2}, \rho\frac{\sigma_\mathrm{y}}{K_\mathrm{IC}}h^{1/2}, V_\mathrm{f}\frac{\sigma_\mathrm{s}}{K_\mathrm{IC}}h^{1/2}, \frac{E w_\mathrm{c}}{K_\mathrm{IC}h^{1/2}}, \frac{b}{h}, \frac{a}{h}\right) = 0 \qquad (\mathrm{Eq.\ 2.8})$$

Remaining valid (Eq.1.3) and (Eq.1.4), another Brittleness number is involved in the problem:

$$N_\mathrm{P} = \rho\frac{\sigma_\mathrm{y}}{K_\mathrm{IC}}h^{1/2} \qquad (\mathrm{Eq.\ 2.9})$$

This latter describes the influence of the bar in the II Stage, the Post-cracking behavior.

Therefore, in the case of RC beams this portion of graph will be described by only (Eq.2.9); on the other hand, the case of HRC would be described by the Reinforcement Brittleness number, being the sum of both contributions of fibres and steel-bar.

Next is represented the values of the brittleness parameters for the plotted numerical curves:

Beam ID	N_P [-]	$N_{P,f}$ [-]	N_w [-]
RC80-6	0.30	0	265
HRC80-6-0.1	0.30	0.17	265
HRC80-6-0.2	0.30	0.34	265
HRC80-6-0.4	0.30	0.67	265
HRC80-6-0.8	0.30	1.34	265
RC80-13	0.53	0	265
HRC80-13-0.1	0.53	0.17	265
HRC80-13-0.2	0.53	0.34	265
HRC80-13-0.4	0.53	0.67	265
HRC80-13-0.8	0.53	1.34	265
RC80-28	1.20	0	265
HRC80-28-0.1	1.20	0.17	265
HRC80-28-0.2	1.20	0.34	265
HRC80-28-0.4	1.20	0.67	265
HRC80-28-0.8	1.20	1.34	265
RC80-50	2.13	0	265
HRC80-50-0.1	2.13	0.17	265
HRC80-50-0.2	2.13	0.34	265
HRC80-50-0.4	2.13	0.67	265
HRC80-50-0.8	2.13	1.34	265

Table 22: Brittleness number of 80 cm depth beams.

As it could be noted, in the Figure 32 and Figure 33 the influence of N_P is so high that the overall behavior is elastic in first stage, linear hardening before the peak and then perfectly plastic before rupture. The influence of the fibres is very low; from a graphical point of view, this fact can be caught because all the simulations tend to shrink to the respective RC curves. The influence of the pull-out is not relevant.

In Figure 30 every specimen has values of brittleness parameters higher than the critical one, so they exhibit a pseudo-hardening behavior in the second stage; but in this plot the influence of fibres is more evident, in fact peaks are very detached. The influence starts to vanish in the Figure 31, in which maximum load are closer.

2.6 Model Performances on RC and HRC

Eventually is performed a performance analysis, in terms of computational time, depending on the two driving parameters: numerical number of fibres and maximum iteration before convergence.

The analysis is performed both for RC beams with different steel-bar reinforcement ratio and HRC with different combination of amount of steel-bar and fibre reinforcement; the selected specimens are: RC40-6, RC40-13, HRC40-13-0.2, HRC40-13-0.8, HRC40-50-0.2 and HRC40-50-0.8. Each one is simulated numerically with 4 kinds of number of numerical fibres (5-10-40-100) and several amounts of bounds on $iter_{MAX}$ (5-10-50-100). Is to be noted that the beams are not tested with a number of fibres equal to its theoretical value, this is due to the very high computational time of several minutes, and the gain in precision and numerical stability is low.

As observed in FRC the change in $iter_{MAX}$, by maintaining constant the number of unknowns (m), doesn't affect the precision and the time of computation is influenced only in the measure of <1%.

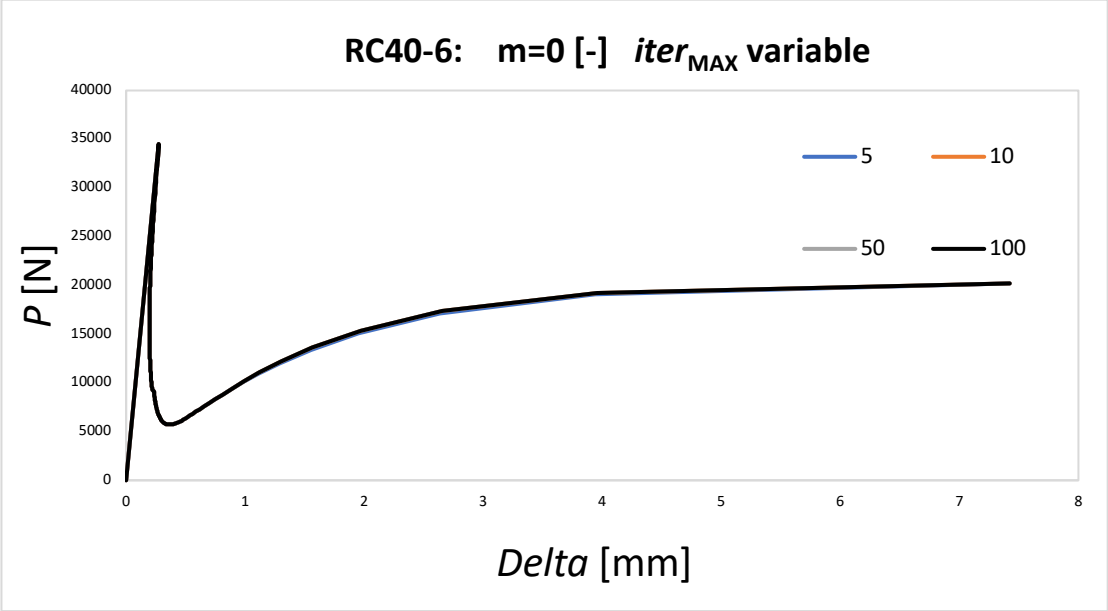

Figure 34: RC40-6 with $iter_{MAX}$ variable.

Beam ID	*m* [-]	$iter_{MAX}$ [-]	*time of execution* [s]
RC40-6	0	5	20.39
RC40-6	0	10	20.67
RC40-6	0	50	20.53
RC40-6	0	100	20.26

Table 23: RC40-6 performances.

The same situation happens for RC40-13, it means varying tensile reinforcement the situation is the same.

An interesting situation can be observed in the case of the HRC beams:

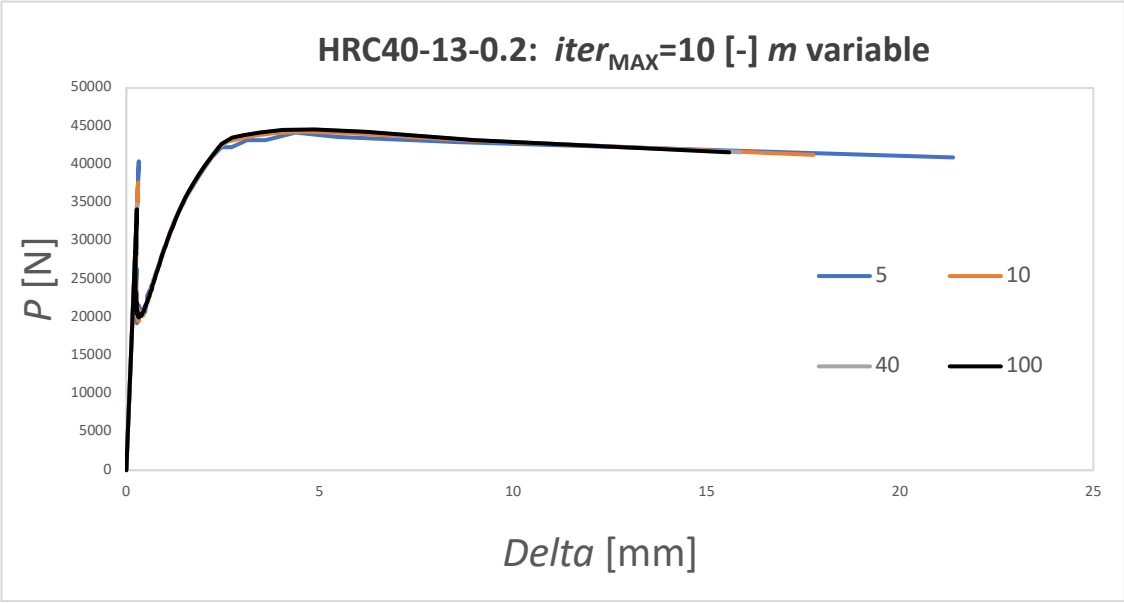

Figure 35: HRC40-13-0.2 with variable m.

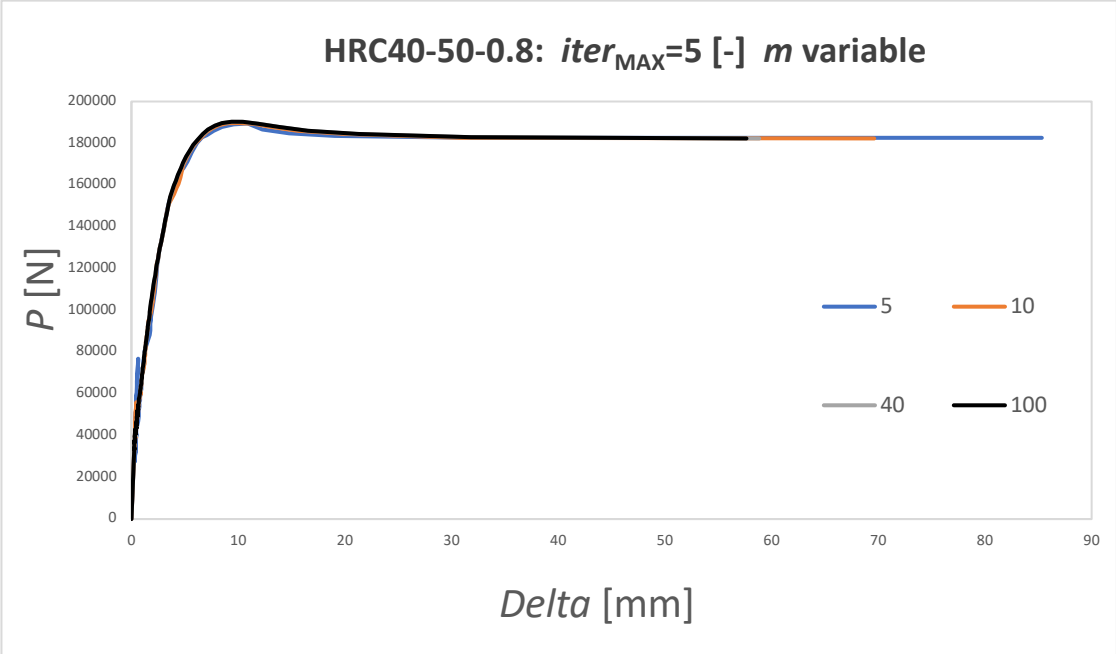

Figure 36: HRC40-50-0.8 with variable m.

By maintaining constant the maximum iteration and varying *m*, the peak and the tail tends to shrink; this is since the higher is the number of unknowns the higher is the numerical stability, therefore increasing m an improvement in precision is gained. As FRC, a trade-off in between precision and time of computation should be found:

Beam ID	*m* [-]	$iter_{MAX}$ [-]	*time of execution* [s]
HRC40-13-0.2	5	5	21.77
HRC40-13-0.2	5	10	21.70
HRC40-13-0.2	5	50	21.80
HRC40-13-0.2	5	100	21.91
HRC40-13-0.2	10	5	22.55
HRC40-13-0.2	10	10	22.46
HRC40-13-0.2	10	50	22.74
HRC40-13-0.2	10	100	22.69
HRC40-13-0.2	40	5	37.11
HRC40-13-0.2	40	10	36.99
HRC40-13-0.2	40	50	36.94
HRC40-13-0.2	40	100	36.80
HRC40-13-0.2	100	5	109.97
HRC40-13-0.2	100	10	110.32
HRC40-13-0.2	100	50	111.05
HRC40-13-0.2	100	100	109.68

Table 24: HRC40-13-0.2 performances.

Beam ID	*m* [-]	$iter_{MAX}$ [-]	*time of execution* [s]
HRC40-50-0.8	5	5	21.81
HRC40-50-0.8	5	10	21.81
HRC40-50-0.8	5	50	21.82
HRC40-50-0.8	5	100	21.92
HRC40-50-0.8	10	5	22.65
HRC40-50-0.8	10	10	22.67
HRC40-50-0.8	10	50	22.59
HRC40-50-0.8	10	100	22.66
HRC40-50-0.8	40	5	36.80
HRC40-50-0.8	40	10	36.76
HRC40-50-0.8	40	50	36.73
HRC40-50-0.8	40	100	36.80
HRC40-50-0.8	100	5	109.72
HRC40-50-0.8	100	10	111.21
HRC40-50-0.8	100	50	109.18
HRC40-50-0.8	100	100	109.28

Table 25: HRC40-50-0.8 performances.

It turns out that once again the suggested number of numerical fibres is 40, being a correct compromise in between precision and speed of computation. Moreover, the number of iterations is not affecting that much the velocity, to be safe always 100 iterations are suggested.

3. Application of the Updated Bridged Crack Model 2.0 (UBCM 2.0) to fibre-reinforced composite materials with non-cementitious matrix

The model deeply described is obviously meant to describe the behavior in flexure of concrete beams, equipped with fibre reinforcement and steel-bar reinforcement. As far as concrete represents a composite material, in this chapter is furnished a preliminary analysis of bending action on composite materials widely use in other field of engineering such as automotive, aerospace and nuclear. Recent studies explain the spread use of fibre-reinforced composite materials, thanks to their incredible light weight and hard strength mixed with great thermal and electrical conductivity features.

The experiments and data analysis are most of the time incomplete and not well representing the reality; from this understanding, the UBCM 2.0 is proposed as an effective tool to investigate properties of fibre-reinforced composites. Here after are discussed many studies covering different materials, composed via a mixture of Polymer, Metal and Ceramic matrices coupled with different fashions of fibre reinforcement.

3.1 Two New Constitutive Laws for fibre-reinforcement.

In the framework of UBCM 2.0 have been introduced two new constitutive laws named *Softening Law,* meant to describe the pull-out of short fibres or rods, and *Hardening Law,* introduced to account for progressing debonding and yielding of continuous fibres. In both cases is present an arbitrary exponent, *n of Ramberg-Osgood* (n_f), driving the passage from stiffening to hardening in the laws, further details are furnished below; it must be identified and represents a user-side input for the code.

The Softening Law, computing the bridging stress at the level of the i-th short reinforcement, is described by the formula:

$$\sigma(w) = \sigma_s \cdot [1 - (\frac{w}{w_c})^{n_f}] \quad \text{(Eq. 3.1)}$$

Where:

- *w:* crack opening displacement [mm]

- σ_s: slippage stress of the fibre [MPa]

- w_c: critical slippage length of the fibre [mm]

- n_f: Ramberg -Osgood exponent [-]

In the following graph is showed the law for many exponent values:

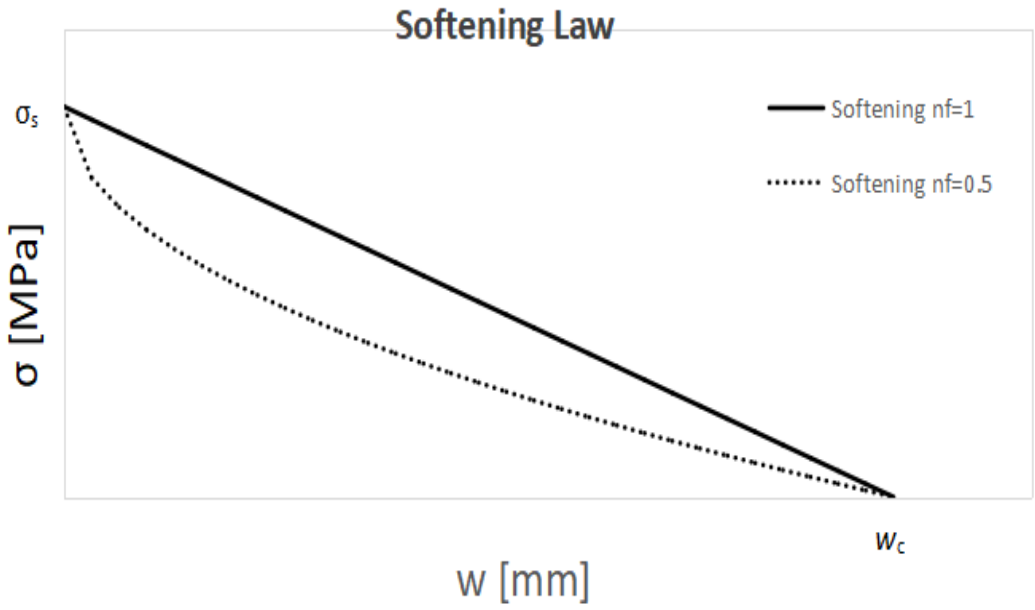

Figure 37: Fibre Softening Law.

As can be deduced from the graph if n_f is equal to 1, the law would present a linear decreasing behavior, changing its value to 0.5 it would behave as a square root function with upper concavity, up to vanish when is equal to zero; in this latter case it would indicate a perfectly brittle rupture of the fibre.

Conversely, the Hardening Law is defined via the formula:

$$\sigma(w) = \sigma_s \cdot \left(\frac{w}{w_c}\right)^{n_f} \qquad \text{(Eq. 3.2)}$$

Here below is represented for different values of n_f :

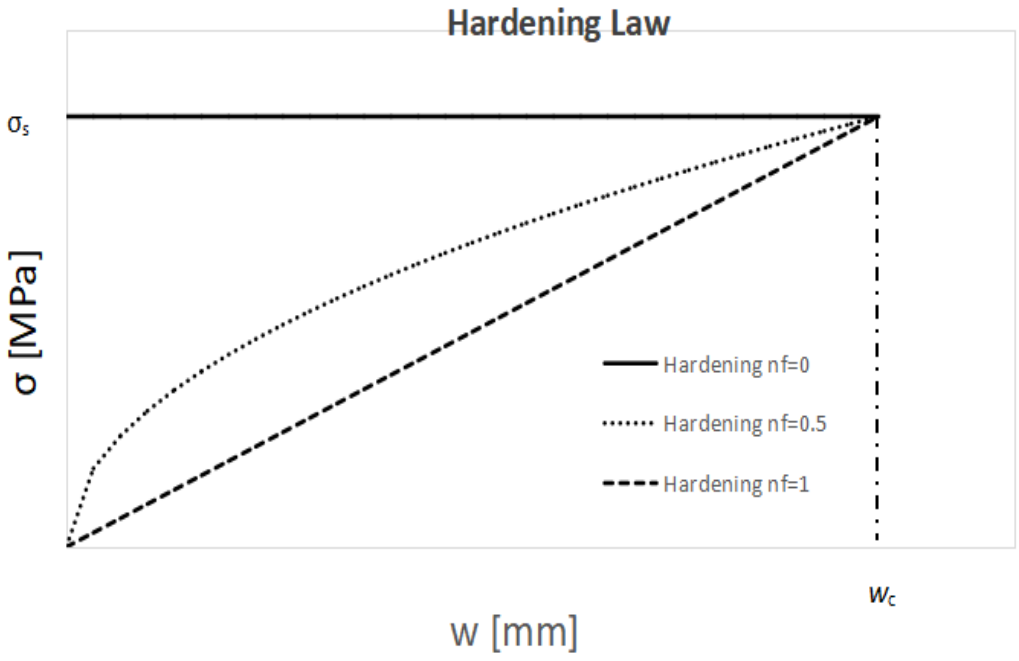

Figure 16: Fibre Hardening Law.

Considering n_f equal to zero, the fibre would exhibit a rigid-perfectly plastic behavior; while if the exponent of Ramberg-Osgood is increased up to 0.5 it would have a hardening branch up to w_c. Eventually, if it is put equal to 1, a linear branch would occur.

3.2 Fibre-reinforced Polymer Matrix Composites (PMC)

According to Zhang et al. [32], Boeing 777 and 787 have up to 50% of their weight composed by Polymer composite, more specifically Carbon Fibre-reinforced Polymers.

This fact underlines the importance of a proper analysis of the above-mentioned material. As a matter of fact, carbon nanotubes possess both high thermal and electrical conductivity letting them be promising low cost electronic and electric wiring [33]. Moreover, their high strength and stiffness yield the possibility to be employed as reinforcement in composite materials. The former paper analyses the tensile and bending behavior of carbon nanotubes reinforced epoxy resin matrix, it will be showed that the model can approximate the results in an effective way.

The matrix is a hot cured epoxy matrix made of three components: bis phenol A epoxy resin (Araldite LY 1564), anhydride hardener (Aradur 917) and amine accelerator (960-1).

The input values for UBCM 2.0 are identified:

EPOXY MATRIX	
Properties	
E (Young's Modulus) [MPa]	2100
K_{IC} (Fracture Toughness) [MPa mm$^{0.5}$]	100

Table 26: Matrix properties of Michalkhan.

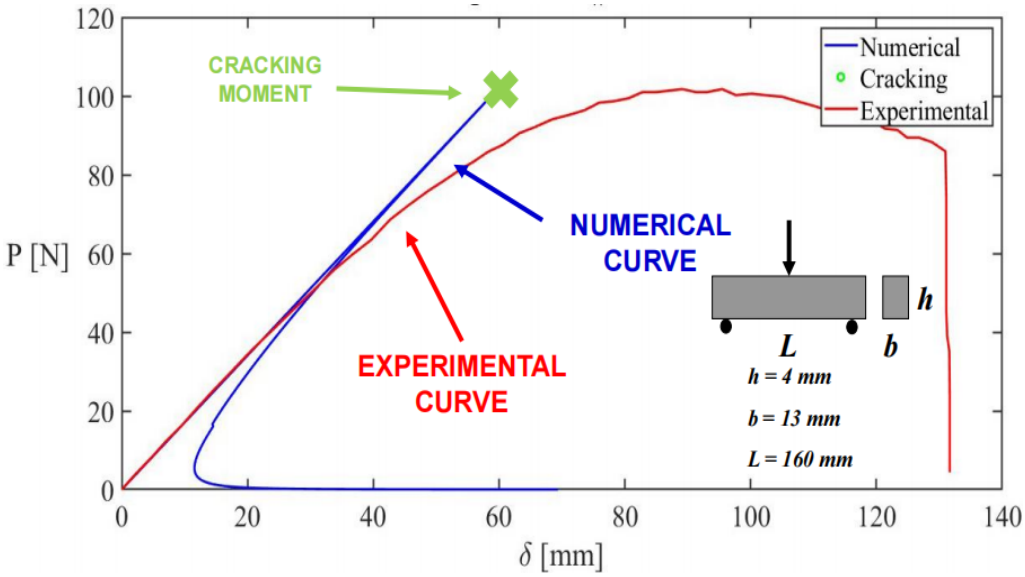

Figure 39: 3-PBT on Michalkhan matrix.

In the above picture is showed the the 3-PBT results and specimen geometry. It can be observed the correct identification of the cracking load and Young`s modulus.

The nanotubes have a diameter of about 8 micron, they are wounded up to create reinforcement fibre of about 200 micron diameter, these latter will provide the bridging actions toughening the composite under bending. Therefore, the specimen considered will be defined as a carbon nanotube fibre reinforced epoxy (CNTF-epoxy) with very high concentration of short reinforcement (V_f = 30 %). As well as done for FRC beams, a detailed identification procedure should be carried out.

Specimen ID	K_{IC} [MPa mm$^{0.5}$]	F_s [N]	w_c [mm]
CNTF-composite	100	6.3	3.2

Table 27: identification for Michalkhan CNTF-composite.

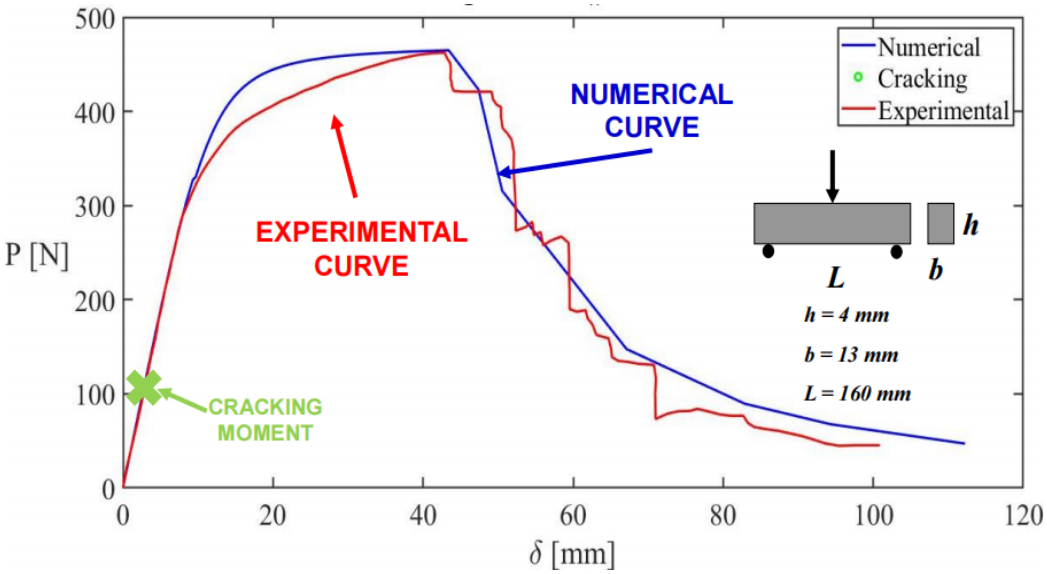

Figure 40: 3-PBT on Michalkhan CNTF-composite.

In this case the numerical results are in good agreement with the experimental one, especially regarding the elastic and the pull-out tail. This result is obtained with a Hardening constitutive law for fibre, with $n_f = 0$, rigid-perfectly plastic.

The second PMC analyzed is from Yao et al. [34], in which the flexural behavior of different Interpenetrating Phase Composite (IPC) specimen is measured by means 3-PBT. The matrix is composed by mainly polyester resin and the short reinforcement are metallic straight filaments, the former component is infiltrated at high temperatures and vacuum conditions into the framework of fibres. These components could be mainly used in structural engineer as components of energy absorption systems.

The interesting fact is that many tests are carried out by varying fibre content, diameter and loading direction leading the characterization of the material as high anisotropic. The identified resin matrix's E is similar to the one indicated (2133 +/- 273 MPa), the specimen's size are h=4 mm, t=10 mm and span S=40 mm;as far as the specimen are unnotched the initial crack size is set equal to *h/50* .The fibre are made of stainless steel with length l_f = 12 mm and two kinds of diameters d_f = 0.09 mm and 0.16 mm. For the sake of precision only the specimen with fibre oriented perpendicularly to the fracture surface has been simulated, denoted as "in-plane" direction, such as to consider the orientation factor of fibre equal to 1. The numerical number of fibres for a good graphical representation is ranging within m= 200 and m= 250. Eventuality, the constitutive Law used is a Softening Law with linear branch (n_f = 1), accounting for pull-out behavior of short fibres. In this table are summarized the values obtained through Identification procedure:

Specimen ID	d_f [mm]	K_{IC} [MPa mm$^{0.5}$]	F_s [N]	w_c [mm]
23.70%-in-plane	0.16	20	3.1	2.5
16.78%-in-plane	0.16	15	2.2	2.5
23.17%-in-plane	0.09	25	1.4	2.3
13.84%-in-plane	0.09	15	1.33	1.95

Table 28: Identification for Yao curves.

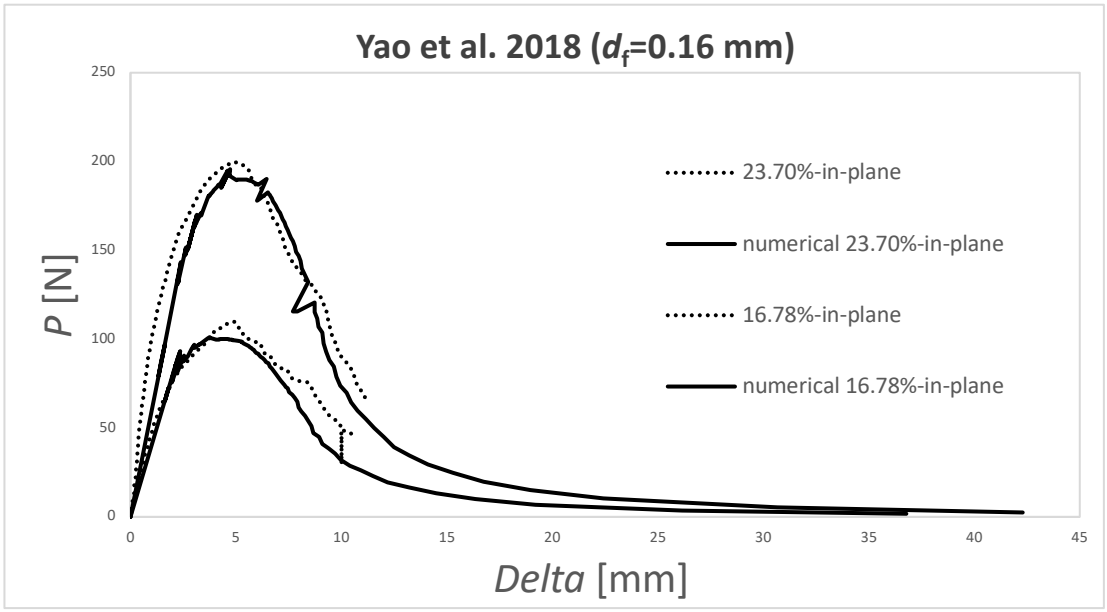

Figure 41: Yao curves with fibre diameter of 0.16 mm.

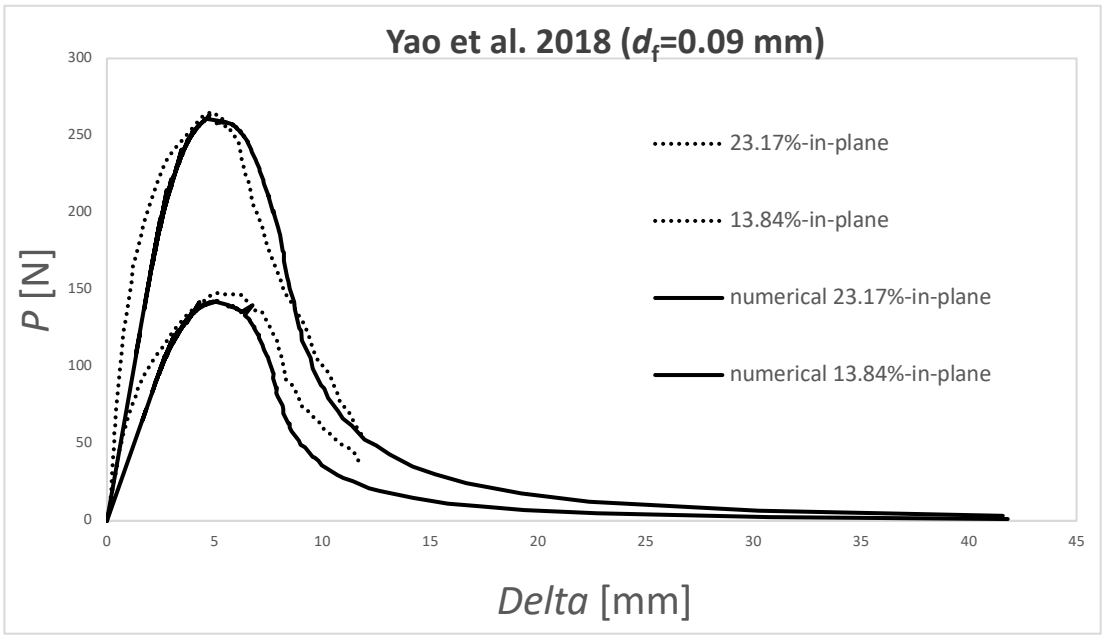

Figure 42: Yao curves for fibre diameter of 0.09 mm.

From previous plots is straightforward to note a great superposition of the curves, underlining quasi-perfect adhesion of the model with experimental curves.

3.3 Fibre-reinforced Metal Matrix Composite (MMC)

Now are considered the composites material having metal matrix and fibre reinforcement that are widely use in the aerospace field. The UBCM 2.0, as described in the preceding chapters, well performs with elastic-perfectly brittle material matrix; under analysis is the scientific paper by Gietl et al. [35], which has the aim to prove the validity of two rule codes, ASTM E399 and ASTM E1820 [36-37] applied to a Tungsten matrix reinforced with Tungsten reinforcement fibres. The scholars want to evaluate the Fracture toughness of this material before and after a heat-treatment, to verify its performance as good plasma-facing shield in future nuclear power plant.

The test performed according to regulation is the 3-PBT, the specimens are notched with initial crack depth *a=1.2-1.7 mm*; the dimensions are: *h*=3-3.5 mm, *t* = 1.3-2.6 mm and the span is *S*= 10 mm. The fibres are oriented perpendicularly to the notch surface and have a length equal to the specimen with a diameter equal to 0.15 mm. The numerical number of fibres is set equal to 250 and the constitutive law is Softening with n_f =1.6; i.e. has a lower concavity decreasing trend up to the identified w_c.

Unfortunately, only the curve related to Specimen 6 is depicted in the paper, these are the results of the identification procedure performed:

Specimen ID	K_{IC} [MPa mm$^{0.5}$]	F_s [N]	w_c [mm]
No. 6 Specimen	750	40	0.2

Table 29: Identification procedure for Gietl curve.

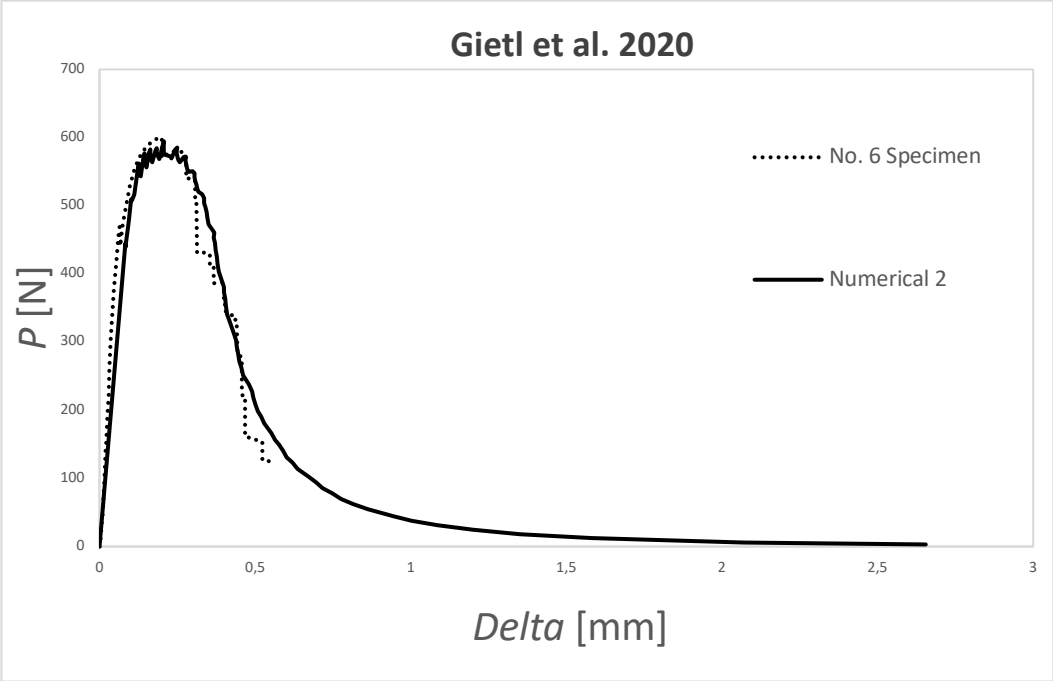

Figure 43: No.6 Specimen Gietl.

Clearly the model can catch the bending behavior of this fibre reinforced MMC; the tail present a descending stair shape representing the debonding of the material at the level of the surface of interaction in between fibres. This latter behavior is nowadays not included in the model but with further research on the topic could be included.

3.4 Fibre-reinforced Ceramic Matrix Composites (CMC)

Eventually the field of Ceramic Matrix Composites (CMC) is tackled. They are characterized by brittle matrix and different kinds of fibre reinforcement.

Owing to their incredible weight reducing properties and high temperature tribological performances, I.e., the interaction between two surfaces, these materials embody an ideal candidate for aeronautics and aerospace structures application [38].

The article analyzed proposes an effective way to model the flexural behavior of long fibre reinforced ceramic matrix woven composites (LFRCWC), by means 4-PBT and acoustic-emission tools to catch the cracking and phase interaction in between fibre and matrix [39].

The framework of the fibre used is called 2.5D and it is composed of two main components: the former is a straight fibre with oval shape cross-section called *warn;* the latter has got wavy shape and wrap the warns and it's called *warp yarn.* The final product turns out to have a woven porous texture in which the silicon dioxide ceramic matrix (SiO_2/SiO_2) can attach via infiltration. The behavior under stress and the property, such as fibre volume fraction, of this fibre reticulum are tricky to be computed; some scholars propose a Finite element method, called *Full-cell model* [40-41], to predict damage behavior and fibre properties. It can be shown that UBCM 2.0 could represent, briefly, a faster and precise method to identify these features of the composite.

During the test campaign 9 unnotched specimens have been tested by means 4-PBT methodology; their dimensions are t=10 mm, h=5 mm and the S=30 mm, the initial crack depth as good practice for uncracked specimen is considered $a=h/50$. The short prisms are tested for different loading direction and fibre orientation, to agree with the framework of UBCM the arrangement which has fibre warn perpendicular to the cracked surface has been chosen, denoted in the paper as A load direction.

As far as no information about the fibre skeleton is given, some hypotheses should be done, also accounting for data found in literature. The diameter is considered d_f=0.5 mm, the length is equal to the span of the element l_f= 30 mm. The numerical number of fibres is put equal to m=300, to achieve a smoother representation in the graphs; eventually, a linear Softening law has been adopted.

The missing variables should be identified, the fibre volume fraction initial values is found in literature V_f = 40%, whereas should be identified via iteration procedure.

Specimen ID	K_{IC} [MPa mm$^{0.5}$]	F_s [N]	w_c [mm]	V_f [%]
No. 2 Specimen	3	6.5	1.8	40

Table 30: Identification procedure for Wang curve.

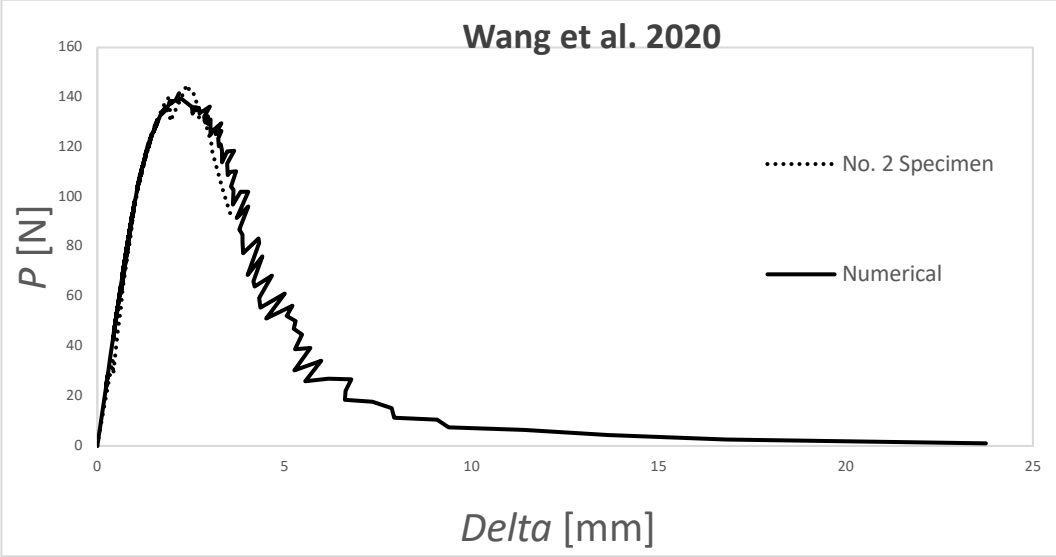

Figure 44: Wang Curve.

Unfortunately, some data are missing, therefore the identification and plot representation is not as accurate as previous studies. Despite this fact, after some assumptions the program can retrieve a good approximation of the experimental results, moreover, could furnish to expert a faster way to identify tricky quantities such as the fibre volume fraction V_f. This latter is usually studied via Finite Element analysis, which it takes long computation and time, resulting as precise as UBCM 2.0 faster method.

Conclusion

The UBCM 2.0 can solve effectively the FRC and PC specimens, by knowing all the input data. It is suggested to put the numerical number of fibres equal to 40 and the $iter_{MAX}$=100, the former affects the most the computational time, while the latter doesn't influence significantly the duration of calculation. However, the most important achievement is that in any case the solution is retrieved in finite time, avoiding convergence problems.

About RC and HRC, the new solution is very effective, but the *n* of Tension-stiffening cannot be retrieved in a closed form yet, further investigation and studies are required. The large test campaign at Shantou University could furnish further data, meanwhile the K-NN algorithm fit with the experimental data identified in literature can offer a reliable starting value for prediction of new specimens. Moreover, the variables *m* and $iter_{MAX}$ could be set as FRC and PC.

Regarding the new materials, the UBCM could represent effectively all the situations; despite this fact, further performance studies should be done both in terms of computational time and precise representation. Since the fibre volume fraction in these cases is higher than concrete, a numerical number of fibres up to 200-300 could be adopted. Eventually in the CMC, the finite element model solution, which compute definition data of the specimens as well, could be substituted by a faster method via identification through UBCM 2.0.

This study opens the door to a new world, UBCM can be generalized and become a benchmark in the flexural analysis of every king of fibre-reinforced materials.

A. New Graphical User Interface for the UBCM 2.0

This Stand-alone application has been completely developed in MATLAB 2022b environment.

A new Graphical User Interface (GUI) has been designed to account for the new features added in the code. In a synthetic way, the added parameters are:

- $iter_{MAX}$: variable for convergence check.

- New constitutive law for HRC and RC beams accounting for Tension Stiffening phenomenon.

- Softening Law and Hardening Law to describe fibre-reinforced composite materials with various matrix.

- Some bugs have been identified and solved.

It turns out that the new app is no more Concrete oriented, but it has the capability to describe properly any kind of fibre-reinforced composite materials.

A.1 Installation

A .zip file would be furnished to the final user ("UBCM2.zip"), it contains three files:

- "UBCM 2.0": which is the stand-alone application.

- MATLAB 2022b runtime.

- a "README'' text file with instructions for the set up in Italian and English languages.

It is suggested to read carefully the text file, afterward the MATLAB runtime should be installed in the PC. Eventually the app UBCM 2.0 could be open and run independently.

A.2 User-side input

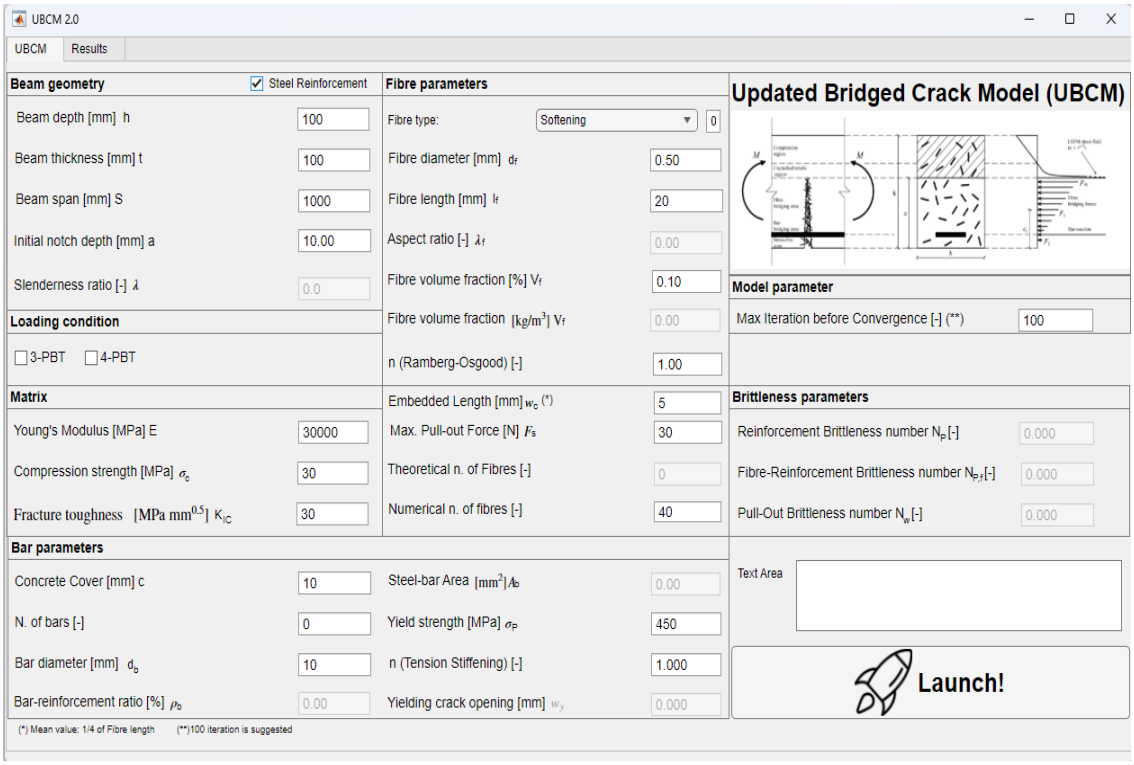

Figure A1: UBCM 2.0 input.

The model is able to represent the flexural behavior in 3-PBT and 4-PBT of: Plain concrete beams, Reinforced concrete beams, Fibre-reinforced beams, Hybrid-reinforced beams and fibre-reinforced composite materials.

The *Beam geometry* table gather all the dimensions of the simulated specimen:

- *h* [mm]: Beam depth.

- *b* [mm]: Beam thickness.

-*S* [mm]: Beam span, distance in between supports.

- *a* [mm]: Initial notch depth, if is faced an unnotched specimen is suggested a value equal to *h/50,* to achieve good adherence with actual results.

Then is asked to choose the *Loading condition,* as mentioned before the choice is in between three-point bending test and four-point test. If by change none of the conditions is selected the code would retrieve an error message.

The *Matrix* is defined by:

- *E* [MPa]: Young's Modulus.

- σ_c [MPa]: Compressive strength, useful to calculate the yielding crack opening displacement in hybrid reinforced concrete. If other type of tests is performed it is useless and could assume any value.

- K_{IC} [MPa $mm^{0.5}$]: Fracture toughness.

If a RC or HRC beam is to be analyzed, the *Bar parameters* should be set properly:

- *c* [mm]: Concrete cover of the beam in the lower edge.

- N. of bars [-]: Number of steel-bars reinforcing the element.

- d_b [mm]: Bar diameter for each reinforcement.

- σ_P [MPa]: Steel-bar yield strength.

- *n (Tension Stiffening)* [-]: Coefficient modelling tension stiffening phenomenon for RC and HRC beams, is a function of scale, fibre content and reinforcement ratio. Should be positive and different from zero, otherwise the code would stop and return an error message. The only suggestion that can be provided before further research is that maintaining constant slenderness ratio and reinforcement ratio, increasing the fibre content *n* should decrease.

To model the fibre reinforcement the table *Fibre parameters* should be filled correctly:

- Fibre type [-]: Constitutive Laws for fibre reinforcement.

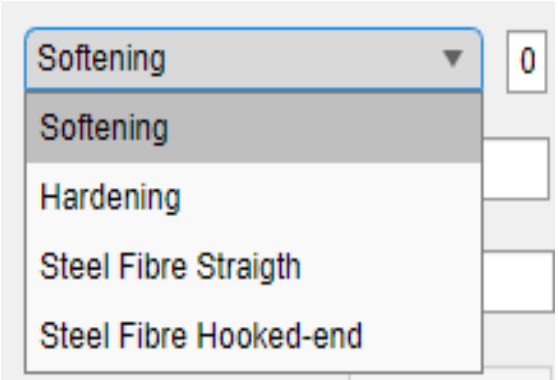

Figure A2: Constitutive Laws for fibre-reinforcement.

The first two laws, *Softening* and *Hardening*, are meant to be used with general fibre-reinforced composite materials. They rely on an exponent called *n (Ramberg-Osgood)*, which control the concavity of the above-mentioned functions; it should be identified and change case by case.

The two laws: *Steel fibre Straight* and *Steel Fibre Hooked-end* could describe properly the typical fibre-reinforcement used in concrete and they do not rely on any coefficient.

- d_f [mm]: Diameter of the fibre.

- l_f [mm]: Fibre length.

- V_f [%]: Fibre volume fraction in percentage.

- *n (Ramberg-Osgood)* [-]: Exponent governing the concavity of Softening and Hardening laws.

- w_c [mm]: Embedded length of the fibre, practically the crack opening displacement at which the short reinforcement is no more effective and no bridges any more the crack surfaces. Nominally equal to 1/4 of the fibre length, is to be identified by the user.

- F_s [N]: Maximum Pull-out force of the single fibre, should be identified.

- *Numerical n. of fibres* [-]: Number of unknowns of the system, to get a smooth representation of the curves should be properly tuned; in case of concrete 40

fibres are enough, in the more general case of fibre-reinforced composite could be greater and reach 300.

Eventually, the tab *Model parameter* manage the tuning of the model. The only variable to be set is the variable mitigating convergence, $iter_{MAX}$. It is suggested to be equal to 100.

It is also present a *Text area* in which the user can note, in a comfortable way, trial values of variable used during identification.

A.3 Model output

Completed the task in A.2, the button" Launch*!"* should be pressed.

The user should pay attention and select on Loading condition, otherwise the following error message would be shown:

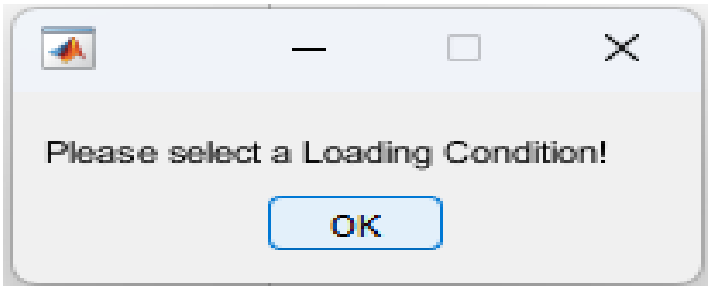

Figure A3: Error message 1.

Then, if a RC or HRC beam is represented, the proper value of *n (Tension Stiffening)* should be selected:

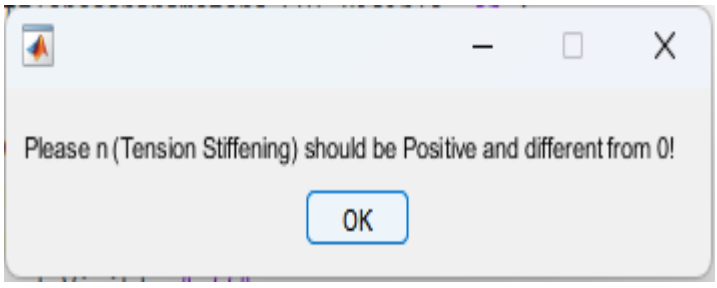

Figure A4: Error message 2.

If the above conditions are not met, the Model would load the data and show with a sliding bar the process computation:

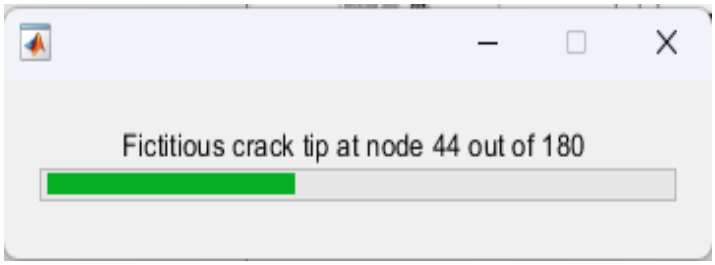

Figure A5: Progress bar.

The output shown would be:

- λ [-]: Slenderness ratio of the specimen.

- ρ_b [%]: Percentage of steel in the cross-section.

- A_b [mm^2]: Steel-bar area.

- w_y [mm]: Yielding crack opening evaluated via Ruiz formula. Accounting only for bi-phase interaction in between concrete and steel.

- λ_f [-]: Aspect ratio of the fibre.

- V_f [kg/m^3]: Fibre volume fraction in kg/m^3.

- *Theoretical n. of fibres* [-]: evaluated via computation by volume.

- N_P [-]: Reinforcement Brittleness number.

- $N_{P,f}$ [-]: Fibre-reinforcement brittleness number.

- N_w [-]: Pull-out brittleness number.

Then in the *Results* page are showed the two graphs: Load [kN] vs Midspan deflection [mm] and Bending moment [kN m] vs rotation [mrad].

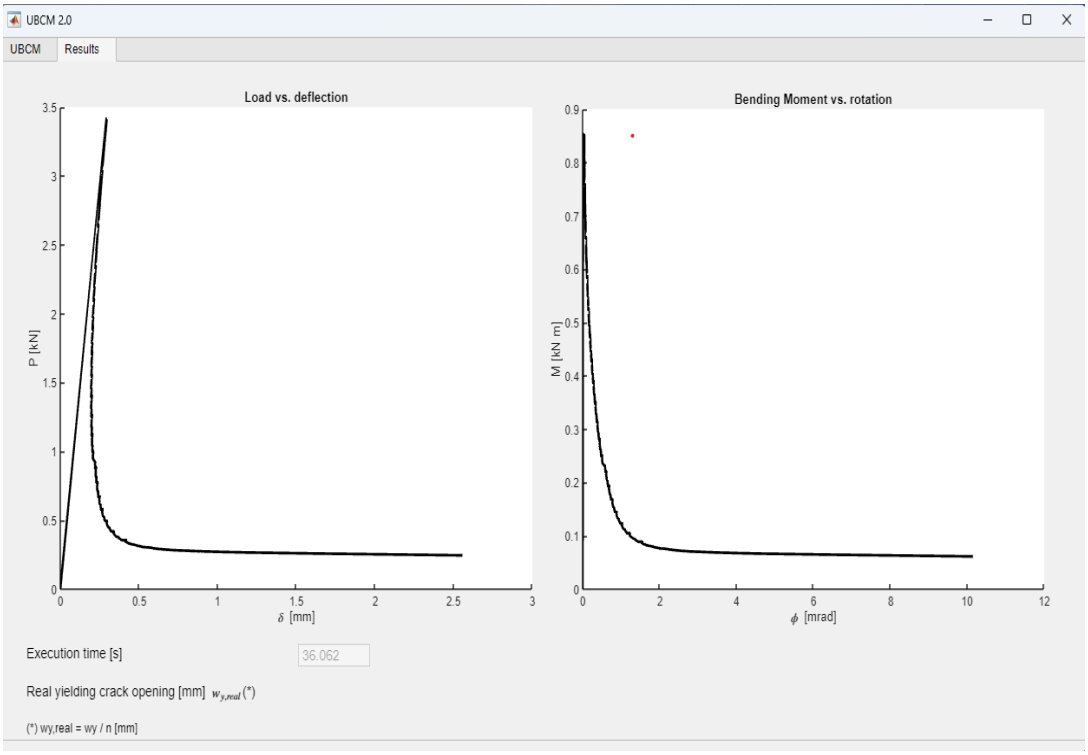

Figure A6: Results page.

Moreover, it can be found the last two results:

- *Execution time* [s].

- $w_{y,real}$ [mm]: Real yielding crack opening, obtained dividing w_y by n of Tension Stiffening.

Once the computation is completed, the execution time would be showed, and the data could be saved in a text file:

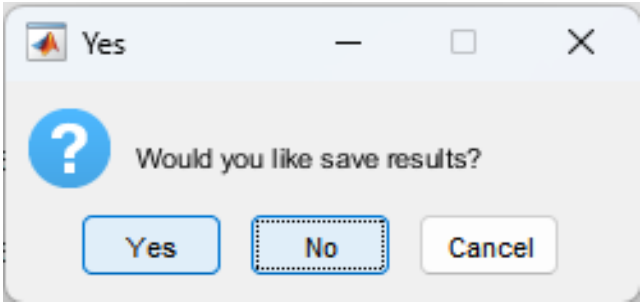

Figure A7: Saving data.

If the user chooses “yes”, should give a name to the text file and could observe the results directly.

CSI: Relative Crack Depth

CSI [-]	w [mm]	Phi [millicad]	M [kNm]	Delta [mm]	P [kN]
0.0000	0.0000	0.0000	0.0000	0.0000	0.0000
0.1000	0.0000	0.0363	0.8537	0.2937	3.4150
0.1050	0.0000	0.0390	0.8341	0.2878	3.3366
0.1105	0.0007	0.0439	0.8512	0.2947	3.4046
0.1150	0.0022	0.0451	0.8104	0.2814	3.2416
0.1200	0.0031	0.0477	0.7907	0.2755	3.1628
0.1250	0.0038	0.0505	0.7738	0.2705	3.0950
0.1300	0.0044	0.0534	0.7582	0.2661	3.0328
0.1350	0.0050	0.0575	0.7591	0.2674	3.0363
0.1400	0.0055	0.0600	0.7388	0.2613	2.9552
0.1450	0.0059	0.0629	0.7238	0.2570	2.8950
0.1500	0.0063	0.0659	0.7102	0.2532	2.8409
0.1550	0.0067	0.0690	0.6976	0.2498	2.7904
0.1600	0.0072	0.0731	0.6958	0.2502	2.7832
0.1650	0.0075	0.0760	0.6815	0.2462	2.7259
0.1700	0.0079	0.0792	0.6693	0.2429	2.6772
0.1750	0.0082	0.0824	0.6580	0.2399	2.6321
0.1800	0.0087	0.0874	0.6610	0.2422	2.6441
0.1850	0.0089	0.0900	0.6450	0.2375	2.5801
0.1900	0.0092	0.0932	0.6336	0.2345	2.5344
0.1950	0.0095	0.0965	0.6233	0.2319	2.4932
0.2000	0.0098	0.0999	0.6137	0.2295	2.4546
0.2050	0.0103	0.1048	0.6134	0.2307	2.4537
0.2100	0.0105	0.1079	0.6020	0.2276	2.4079
0.2150	0.0108	0.1113	0.5923	0.2253	2.3693

Figure A8: Results saved in the text file.

References

1. Carpinteri A (1981) A fracture mechanics model for reinforced concrete collapse. In: Proceedings of the IABSE colloquium on advanced mechanics of reinforced concrete, Delft.
2. Carpinteri A (1984) Stability of fracturing process in RC beams. J Struct Eng ASCE 110(3): 544-558.
3. Bosco C, Carpinteri A (1995) Discontinuous constitutive response of brittle matrix fibrous composites. J Mech Phys Solids 1995;43(2):261-74.
4. Rubino A, Accornero F, Carpinteri A (2023) Flexural behavior and minimum reinforcement condition in hybrid-reinforced concrete beams. Struct Conc, fib Wiley 2023;1-12.
5. Accornero F, Rubino A, Carpinteri A (2022) Post-cracking regimes in the flexural behaviour of fibre-reinforced concrete beams. Int J of Sol and Struct. Elsevier.
6. Accornero F, Rubino A, Carpinteri A (2022) A fracture mechanics approach to the design of hybrid-reinforced concrete beams. Eng Fract Mech. Elsevier.
7. Carpinteri A (1981) Static and energetic fracture parameters for rocks and concretes. Mat and Cons. Springer.
8. Rubino A (2023) A fracture mechanics approach to the design of fibre-reinforced and hybrid-reinforced concrete structures. Doctoral dissertation, Turin.
9. RILEM TC 162-TDF (2002) Test and design method for steel fibre reinforce concrete. Bending test. Final recommendation. Mater Struct 2002;35(9):579-82.
10. Buckingham E (1914) On physically similar systems; illustrations of the use of dimensional equations. Phys Rev 4(4);345.

11. Yoo D, Gohil U, Gries T, Yoon Y (2015) Comparative low-velocity impact response of textile-reinforced concrete and steel-fiber-reinforced concrete beams. J of Comp Mat 0(0):1-11.

12. Bencardino F (2013) Mechanical parameters and post-cracking behaviour of HPFRC according to three-point and four-point bending test. Adv in Civ Eng . Hindawi.

13. Nilson, Arthur H (1968) Nonlinear analysis of reinforced concrete by the finite element method. ACI J. Proceedings V.65(9):757-66.

14. Model Code (2010) The final draft of the fib MC2010. Federation International du Beton fib. Chapter 6.

15. Stramandinoli R.S.B, La Rovere H.L (2008) An efficient tension-stiffening model for nonlinear analysis of reinforced concrete members. Eng Struct 30(2008): 2069-80.

16. CEB (1985) Cracking and deformation. Bulletin d`information N.158. Paris, France.

17. Torres LI, Lopez F, Bozzo L.M (2004) Tension-stiffening model for cracked flexural concrete members. ASCE 0733-9445(2004)130:8(1242).

18. Ding Y, Ning X, Zhang Y, Pacheco F, Aguilar J.B (2014) Fibres for enhancing of the bond capacity between GFRP rebar and concrete. Cons and Buil Mat 51:303-12. Elsevier.

19. Chao S.H, Naaman A.E, Parra G..J (2010) Local bond stress-slip models for reinforcing bars and prestressing strands in high-performance fiber-reinforced cement composites. ACI J 272:151-72.

20. Hameed R, Turatsinze A, Duprat F, Sellier A (2013) Bond stress-slip behaviour of steel reinforcing bar embedded in hybrid fiber-reinforced concrete. KSCE J of Civ Eng (2013) 17(7):1700-7.

21. Soranakom C, Mobasher B (2010) Modeling of tension stiffening in reinforced cement composites: part I. theoretical modeling. Mat and Struct (2010) 43:1217-30.

22. Fantilli A.P, Gorino A, Chiaia B. (2018) Multi-scale tension stiffening approach for the minimum reinforcement of hybrid concrete beams. Comp Mod of Conc Struct (2018). Taylor & Francis.

23. Ruiz G, Elices M, Planas J (1999) Size effects and bond-slip dependence of ligthly reinforced concrete beams. Eur Struct Int Soc 1999;24:67-97.

24. Holshemacher K, Mueller T, Ribakov Y (2010) effect of steel fibres on mechanical properties of high-strength concrete. Mater Des 2010; 31(5):2604-15.

25. Oliveira E, Nunes B (2024) Application of high strength steel fiber-reinforced concrete to reduce the use of conventional rebars in normal-strength reinforced concrete beams. Rev Cad Ped v.21, n.10:1-29.

26. Seara S, Gonzalez B, Martinez F, Eiras J (2018) Flexural performance of reinforced concrete beams made recycled concrete coarse aggregate. Eng Struct 156 (2018) 32-45.

27. Altun F, Haktanir T, Ari K (2007) Effects of steel fiber addition on mechanical properties of concrete and RC beams. Cons and Build Mat 21 (2007) 21:654-61.

28. Conforti A, Zerbino R, Plizzari G (2020) Assessing the influence of fibers on the flexural behavior of reinforced concrete beams with different longitudinal reinforcement ratios. Struct Conc 2020;1-14.

29. Li X, Pei S, Fan K, Geng H, Li F (2020) Bending performance of steel fiber reinforced concrete based on composite-recycled aggregate and matched with 500 MPa rebars. Materials 2020,13,930.

30. Hasgul H, Turker K, Birol T, Yavas A (2018) Flexural behaviour of ultra-high-performance fiber reinforced concrete beams with low and high reinforcement ratios. Struct Conc 2018; 1-14.

31. Murphy K.P (2012) Machine learning: a probabilistic perspective. MIT press.

32. Zhang X, Chen Y, Hu J (2018) Recent advances in the development of aerospace materilas. Prog in Aer Sci 97(2018) 22-34.

33. Mikhalchan A, Gspann T, Windle A (2016) Aligned carbon nanotube-epoxy composites: the effect organization on strength, stiffness, and toughness. J Mat Sci 2016 51:10005-25.

34. Yao B, Zhou Z, Duan L, Chen Z (2018) Characterization of three-point bending properties of metal-resin interpenetrating phase composites. RSC Adv (2018) Issue 29.

35. Gietl H, Olbrich S, Riesch J, Holzner G, (2020) Estimation of the fracture toughness of tungsten fibre-reinforced tungsten composites. Eng Frac Mec 232.

36. ASTM (2013) E1820-09 Standard test method for measurement of fracture toughness.

37. E399-90 Standard test method for plane-strain fracture toughness of metallic materials.

38. Wei J, Lin B, Cao X, Zhang X, Fang S (2015) Two-dimensional evaluation of 3D needled C_f/SiC composite fiber bundle surface. App Surf Sci 355(2015) 166-70.

39. Wang H, Wang Y, Lin B, Wei J, He Y (2019) What roles do ceramic matrix and woven fibers have in bending strength of SiO_2/SiO_2 composites: An experimental investigation and acoustic emission analysis. Cer Int 45 (2019) 1143-49.

40. Song J, Wen W, Cui H, Zhang H, Xu Y (2016) finite element analysis 2.5D woven composites, Part I: Microstructure and 3D finite element model. Appl Comp Mater (2016) 23:29-44.

41. Wang N, Wen W, Cui H (2021) A continuum damage model for fatigue life prediction of 2.5D woven composites. Sci and Eng of Comp Mat (2021) 28:653-67.

42. Carpinteri A (2017) Advanced structural mechanics. CRC press.

43. Carpinteri A (2021) Fracture and complexity: One century since Griffith's milestone. Springer.

44. Bosco C, Carpinteri A, Debernardi P.G (1990) Minimum reinforcement in high-strength concrete. J of Struct Eng 116(2), ASCE.

45. Carpinteri A, Massabo` R (1996) Bridged versus cohesive crack in the flexural behavior of brittle-matrix composites. Int J Fract 81(2):125-145.

Ringraziamenti